Immune privilege of adipocyte mitochondria protects from obesity

Anh Cuong Hoang
Ulm University
Haidong Yu
Ulm University
Ya-Tin Lin
Chang Gung University https://orcid.org/0000-0001-7910-1223
Jin-Chung Chen
Chang Gung University
Chia-Chun Chen
Chang Gung University
Victoria Diedrich
Ulm University
Annika Herwig
Ulm University
Kathrin Landgraf
University of Leipzig, Pediatric Research Centre, Department of Women's and Child Health
https://orcid.org/0000-0002-6878-6033
Antje Körner
Center for Pediatric Research Leipzig (CPL), University Hospital for Children & Adolescents, University of Leipzig, Leipzig https://orcid.org/0000-0001-6001-0356
Tamás Roszer (tamas.roeszer@uni-ulm.de)
Ulm University

Article

Keywords: innate immunity, obesity, interferons, IFI16, vitamin D

Posted Date: November 4th, 2021

DOI: https://doi.org/10.21203/rs.3.rs-988599/v1

Additional Declarations: There is **NO** Competing Interest.

Version of Record: A version of this preprint was published at Nature Metabolism on November 28th, 2022. See the published version at https://doi.org/10.1038/s42255-022-00683-w.

Immune privilege of adipocyte mitochondria protects from obesity

Anh Cuong Hoang[1]; Haidong Yu[1], Ya-Tin Lin[2], Jin-Chung Chen[2], Chia-Chun Chen[3], Victoria Diedrich[1], Annika Herwig[1], Kathrin Landgraf[4], Antje Körner[4], Tamás Röszer[1*]

[1]Institute of Neurobiology, Ulm University, Ulm, Germany

[2]Department of Physiology and Pharmacology, Graduate Institute of Biomedical Sciences, School of Medicine; Healthy Aging Research Center, Chang Gung University, Taiwan

[3]Molecular Medicine Research Center, Chang Gung Memorial Hospital at Linkou, Taiwan

[4]Center for Pediatric Research, University Hospital for Children and Adolescents, University of Leipzig, Germany

*Correspondence to: tamas.roeszer@uni-ulm.de, Fax: +49 (0) 731-50-22629

Short title: Anti-mitochondrial immune response aggravates obesity

Key words: innate immunity – obesity – interferons – IFI16 – vitamin D

Abstract

Infant nutrition is rich in lipids, and the adipose tissue has been adapted to properly break down neutral lipids and oxidize fatty acids in infancy. Accordingly, infant adipose tissue contains so-called beige adipocytes, which burn off lipids to heat, and impede fat storage and obesity. We show here that infant adipocytes are immune privileged sites for mitochondria due to a blockade in interferon regulatory factor 7 (IRF7)-signaling, which allows mitochondrial RNA to trigger beige adipocyte differentiation through mitochondria-to-nucleus signaling. These mechanisms serve to maintain an extensive mitochondrial network in beige adipocytes and protect against obesity. By contrast, fat storing white adipocytes lack these mechanisms and respond to their mitochondrial content with inflammation. We show that obesity subverts the immune privilege for mitochondria in adipocytes, which reduces mitochondrial mass and abrogates beige adipocyte development. In turn, suppressing IRF7 signaling and restoring the RNA-mediated mitochondria-to-nucleus signaling in adipocytes effectively reduces obesity.

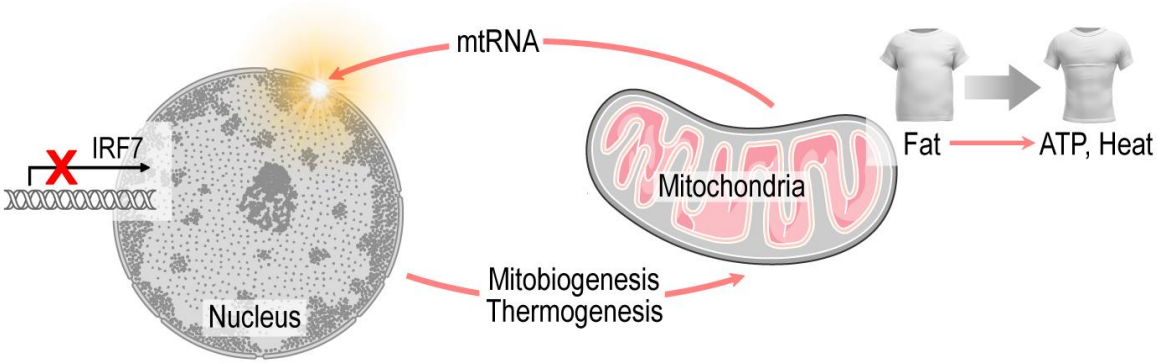

Graphical Abstract

Infant adipocytes have a suppressed IRF7 expression and a mitochondria-to-nucleus signaling through mitochondrial RNA (mtRNA), which stimulates the transcription of beige adipocyte genes, and is key for mitobiogenesis and burning off fat as heat.

Video summary

https://figshare.com/s/36e7ca6a4953471fba42

Childhood obesity is a serious public health crisis and is associated with an increased risk of obesity and diabetes in adulthood, which is projected to affect ~58% of the world's adult population by 2030 (1-3). Obesity is an excessive accumulation of white adipose tissue (WAT) mediated by a mismatch between energy supply and utilization. Infant nutrition is rich in lipids, and adipocytes in the infant WAT break down lipids to free fatty acids, and generate energy and heat from lipids in their extensive mitochondrial network (4-6). These fat oxidizing and thermogenic fat cells are termed as beige adipocytes (7, 8). In adults however, adipocytes of the subcutaneous fat depots are scarce in mitochondria and accumulate fat (9, 10). WAT is necessary for metabolic and endocrine health in adulthood, however its excess expansion accounts for metabolic diseases (1-3). Previous studies have suggested that the premature loss of fat oxidizing and thermogenic potential in infant WAT is accelerated in childhood obesity (2, 3, 10), and delaying or reverting the metabolic shift of WAT from fat catabolism to storage has therapeutic potential in the prevention of obesity (7, 8).

Cell metabolism of fat into ATP and heat requires an extensive mitochondrial network and mitochondrial uncoupling (8), which increases the abundance of "misplaced" mitochondria-associated danger signals in the cytoplasm, such as prokaryote-type mitochondrial DNA (mtDNA) and virus-like double stranded RNA (dsRNA). These signals trigger inflammasome activation and interferon (IFN) response (11), which abrogate the expansion of the mitochondrial network and the capacity of fat oxidation, and cause metabolic inflammation (12). Obesity is a hyper-inflammatory disorder, and IFNs trigger obesity-associated metabolic diseases (13, 14), especially in children with insufficient breastfeeding (15), who are prone for premature WAT expansion (7).

These observations prompted us to question whether infant adipocytes have a unique nucleic acid immunity that supports their mitochondrial network. We found that the infant

subcutaneous adipocytes were immune privileged towards mitochondria due to the suppression of cytosolic mtDNA recognition and interferon regulatory factor 7 (IRF7). Mitochondrial RNA (mtRNA) eventually activated a mitochondria-to-nucleus signaling which stimulated mitobiogenesis and beige adipocyte development without provoking an IFN-response against mitochondrial content. These mechanisms were lacking from the adult subcutaneous adipocytes, which responded with IFN-burst to mitochondrial content and were hostile for mitochondria. Obesity subverted mitochondrial immune privilege in adipocytes, and in turn, restoring mtRNA-mediated signaling effectively reduced obesity. Innate immune sensing of mitochondrial nucleic acids is hence a novel mechanism which controls early adipose tissue development and protects against obesity.

Results

Infant subcutaneous fat is immune privileged for mitochondria

After birth, subcutaneous adipose tissue is a relevant fat depot in mouse and human (6), hence we surveyed the transcriptional landscape of mouse inguinal adipose tissue (iAT) at postnatal day 6 (P6) and P56 by next-generation sequencing (NGS) (Fig. S1A, Fig. S2A,B). P6 iAT was rich in beige adipocytes and mtDNA, and expressed beige adipocyte-associated transcripts together with *Prdm16*, encoding PR domain containing 16, a key transcriptional regulator of thermogenic fat development (Fig. S1B-E) (10, 16). By contrast, P56 iAT lacked beige adipocytes, contained significantly lower amounts of mtDNA, and expressed transcripts associated with white adipocytes (Fig. S1B-E). Thus, infant but not adult mouse fat is rich in thermogenic, fat-oxidizing adipocytes (6). Beige adipocytes have been reported in the subcutaneous adipose tissue of human infants and children (7, 10), and we found that the level of *UCP1*, encoding uncoupling protein 10, in human

infant iAT correlated positively with the level of beige adipocyte genes and negatively with white adipocyte markers (Fig. S1F).

IFN-stimulated genes (ISGs) were suppressed in adipocytes at P6 (Fig. 1A-C), and the under-represented ISGs belonged to one network (Fig. S2B), and included the stimulator of interferon genes (STING) and IFN-inducible protein absent in melanoma 2 (AIM2) pathways (Fig. 1B). These pathways trigger DNA-inflammasome assembly, inflammasome activation and IFN-response to cytosolic DNA (17). Cytosolic B-DNA is recognized by DDX41 (DEAD-box helicase 41) and p204, also known as IFNγ-inducible protein 204 (IFI204) in BALB/C mice, IFI205 in C57/BL6 mice, and IFI16 in human (17) (for details see Fig. S2C). Cytosolic Z-DNA, which is prevalent in transcriptionally active cells (18), is recognized by ZBP1 (Z-DNA-binding protein 1, also termed DAI (19)). Transcription of these cytosolic DNA sensors was low at P6, specifically in adipocytes (Fig. 1B,C, Fig. S2D-H).

The STING and AIM2 pathways converge on interferon regulatory factor 3 and 7 (IRF3, IRF7), and the adipocyte level of *Irf7* was significantly lower at P6 than at P56 (Fig. 1B,C). Accordingly, P6 adipocytes were protected from inflammasome activation by cytosolic DNA (Fig. 1B, Fig. S3A-D, S4A-C) or endosomal DNA (Fig. S5A-F), and genetic ablation of IRF7 protected adipocytes from IFN-response against mtDNA (Fig. S4E). IRF7 activation triggered the expression of the STING/AIM2 pathway in P56 adipocytes (Fig. S4F), and consistently, the STING/AIM2 pathway proteins were lacking in P6 adipocytes (Fig. 1D). In turn, AIM2, DDX41, p204 and ZBP1 were present in the perinuclear region and in the cytoplasm of P56 adipocytes, which distribution is consistent with their known tasks to monitor DNA fragments in specific subcellular compartments (Fig. 1D) (19, 20).

We next examined the expression of the STING/AIM2 pathways and IRF7 in the inguinal adipose tissue (iAT) of human infants and children (0.3–6.9 years of age, N=26). Overweight (BMI-SDS>1.28) and obesity (BMI-SDS>1.88) strongly increased the expression of *IFI16*, *ZBP1*, and *IRF7*, and moderately increased *TMEM173* level (Fig. 1E, S6A-C), which was coherent with the loss of beige adipocytes in childhood obesity (3, 7, 21). IFI16 protein level positively correlated with adipocyte size (Fig. 1E). IRF7 and IFI16 expression was triggered by *in vitro* white adipogenesis (Fig. 1E, Fig. S6D), and *TMEM173* expression positively correlated with *IFI16* and *IRF7* levels and was increased by premature loss of beige fat (Fig. 1E, Fig. S6D). We next extended the age group of our analysis (7.0–11.0 years, N=73; 11.1–20.5 years, N=155) and found that in lean subjects the STING/AIM2 pathways moderately increased with age, matching the time scale of the physiological WAT expansion (Fig. S6E).

In summary, immune response to cytosolic mtDNA and mtRNA was lacking in P6 adipocytes and was dependent on IRF7 (Fig. 1F, Fig. S3D, Fig. S4C-E). Moreover, STING had opposing functions in P6 and P56 adipocytes: activation of STING with its natural activator 2'3'-cyclic-GMP-AMP (cGAMP), increased autophagosome number and mitophagy in P6 adipocytes (Fig. 1G,H,I, Fig. S7A-C), while STING inhibition compromised mitophagy, reduced mitochondrial mass and led to inflammation in P6 adipocytes (Fig S7D-G). On the contrary, cGAMP triggered IFN-response in P56 adipocytes (Fig. 1F, Fig. S3D).

STING stimulates IFN-response against mtDNA (22), however it is known that the STING signaling may also induce autophagy (23, 24). Mitophagy is a form of autophagy and protects the cytosol from leaking mtDNA (25). Our data show that an autophagy-inducer effect of STING protects from cytosolic mtDNA accumulation in infant adipocytes (Fig. S7D-G), and infant adipocytes are also protected against the STING-induced IFN-response (Fig. 1I).

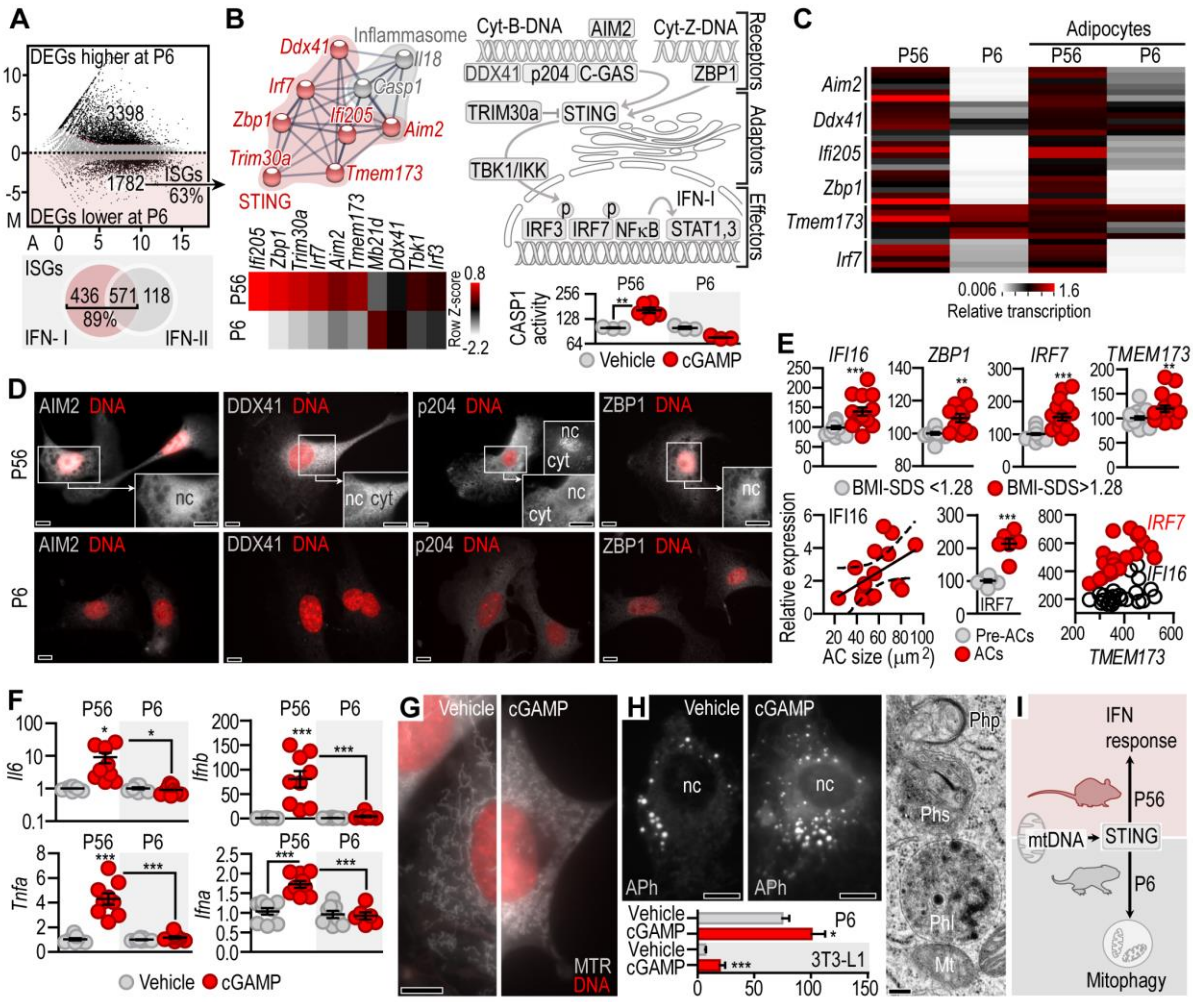

Fig 1. Infant adipocytes are immune privileged for mitochondria

(**A**) NGS analysis of mouse iAT, DEGs: differentially expressed genes, ISGs: interferon stimulated genes. (**B**) Excerpt of the interactome-, and heat map of genes underrepresented in P6 iAT. Scheme of STING signaling, and inflammasome-associated caspase 1 (CASP1) activity in P6 and P56 iAT in response to 18h cGAMP treatment. Cyt-B-DNA: cytosolic B-DNA; Cyt-Z-DNA: cytosolic Z-DNA. (**C**) Transcription of the STING/AIM2 pathways in mouse iAT at P6 and P56. (**D**) Expression of DNA sensors in adipocytes. (**E**) Transcription of the STING/AIM2 pathway in iAT of human infants and children. Correlation of IFI16 level and adipocyte (AC) size in human. IRF7 level in human preadipocytes (Pre-ACs) and white ACs. Correlation of *IFI16* and *IRF7* with *TMEM173* levels in human infant iAT. (**F**) Response of P6 and P56 adipocytes to 18h cGAMP treatment. (**G**) Mito-Tracker-Red (MTR) staining of P6 adipocytes after 2h cGAMP treatment. (**H**) *Top:* Labeling of autophagosomes (APh) in P6 adipocytes. nc: nucleus, *Bottom:* APh number in P6 adipocytes and in 3T3-L1 cells following vehicle or 2h cGAMP treatment. TEM image of a P6 adipocyte showing autophagosome formation. Php: phagophore, Phs: phagosome, Phl: phagolysosome, Mt: mitochondrion. Scale: 10 μm (D,G,H); 0.1 μm (TEM). **P*<0.05, ***P*<0.01, ****P*<0.001. Student's 2-tailed unpaired *t*-test or one-way ANOVA with Dunnett's post-hoc test. (**I**) Opposing effects of STING activation in P6 and P56 iAT.

127

Infant adipocytes employ mtRNA as a paracrine signal for beige fat development

We found that P6 adipocytes secreted mitochondrial contents in extracellular vesicles (EVs). Adipocyte EVs were generated in the endosomal pathway, by inverse budding of endosomes, leading to the formation of multivesicular bodies (MVBs) (Fig. 2A,B; S8A-G). In line with this, transcripts necessary for inverse budding of endosomes and the generation of MVBs were over-represented in iAT at P6 (Fig. 2B). Inverse budding allows cytosolic nucleic acids to be delivered to MVBs, and this process is a form of micro-autophagy (26). Endosomal content can be further targeted for degradation in the lysosomes; however lysosomal genes were underrepresented in P6 iAT and by contrast, transcripts required for exocytosis were over-represented in P6 iAT (Fig. 2B). P6 EVs were packed with mtDNA molecules and mitochondrial mRNA and rRNA species (Fig. 2C-E). Some of the EV cargo mRNAs, including *Nd5*, *Co1* and *Cytb*, are known to generate non-coding mtRNA species (27, 28). The adipose tissue mesenchymal stem cell EV-specific microRNA miR29a-5p was absent in P6 EVs (Fig. S8H). P6 EVs also contained minimal amounts of circular-RNA, piwi-RNAs and the adipocyte-specific microRNA miR34a, together with traces of *Ucp1* mRNA (Fig. S8I). P6 adipocytes released more EVs than their P56 counterparts (Fig. S8J), and inhibitors of EV generation suppressed both DNA and RNA release from adipocytes (Fig. S8K).

P6 EVs increased mitochondrial content, mitobiogenesis, uncoupling protein-1 (UCP1) expression and thermogenesis in recipient adipocytes, without inducing unfavorable mitochondrial swelling (Fig. 2F,G; Fig. S9A). P6 EVs also triggered the transcription of beige adipocyte genes (Fig. 2H). Adipocyte EVs carried dsRNA (Fig. 2E, S9B), which may activate Toll-like receptor 3 (TLR3), or the retinoic acid-inducible gene-I (RIG-I) and RIG-I-like melanoma differentiation-associated protein 5 (MDA5) signaling (29, 30). Cytosolic single stranded RNA, or stimulation of

TLR3 did not mirror the effects of EVs (Fig. S10A-C), unlike the activation of RIG-I/MDA5 which induced strong beige adipocyte gene transcription (Fig. 2I, S10D-H).

Beige-inducing effect of EVs was dependent on IL-6/STAT3 and RIG-I/MDA5 signaling (Fig. 2J, Fig. S11A-E), and the lack of RIG-I or MDA5 led to the loss of beige adipocytes and compromised mitobiogenesis, and compromised the expression of the nucleus-encoded mitochondrial succinate dehydrogenase complex (Fig. 11F,G).

Nucleic acids in EVs are protected from extracellular nucleases by the surrounding membrane and they may function as intercellular messengers (31). Accordingly, delivery of total mtRNA into the cytosol induced beige adipocyte gene expression, mitobiogenesis and mitochondrial thermogenesis (Fig. 2I, Fig. S10G,H) in a RIG-I/MDA5-dependent manner (Fig. 2J,K, Fig. S11H). Cytosolic mtDNA stimulated mitophagy in infant adipocytes (Fig. S12A,B). In summary, EVs of infant adipocytes conveyed mtRNA and mtDNA to recipient adipocytes and triggered beige adipocyte differentiation and mitophagy, respectively.

Breast milk is a known beige-inducing signal (7), and we found that human breast milk EVs were rich in mtRNA (Fig. S12C). Eventually, breast milk EVs – unlike formula milk EVs – induced beige adipocyte gene expression, mitobiogenesis and mitochondrial thermogenesis, and in turn reduced IRF7 abundance in human adipocytes (Fig. S12D,E).

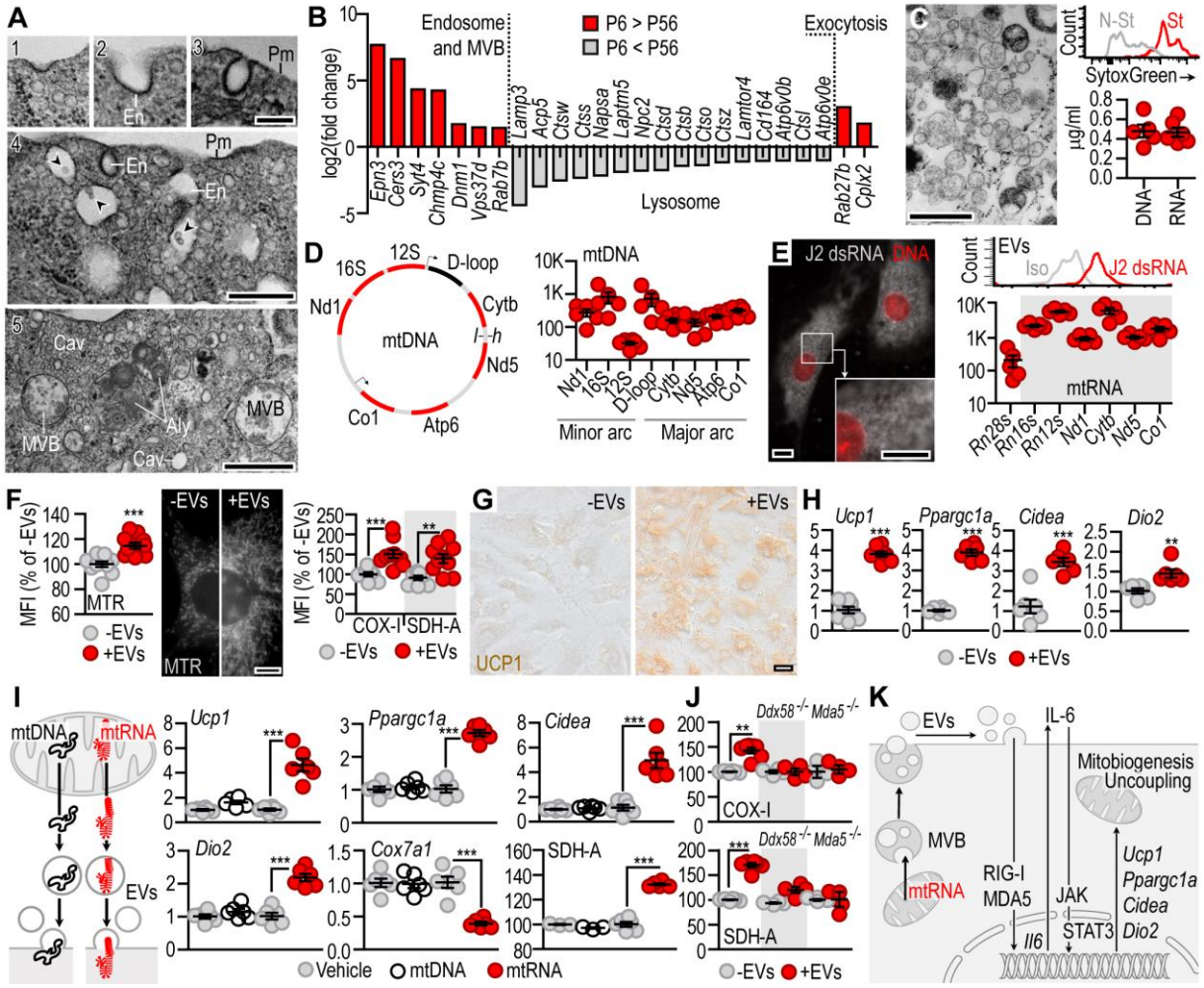

Fig. 2. Infant adipocytes cast away mtRNA to induce beige adipose tissue development
(**A**) Clathrin-coated pits, endosome budding [1–4] and multivesicular bodies (MVBs) [5] in P6 adipocyte. Pm: plasma membrane, En: endosome, Aly: autolysosome, Cav: caveolae, arrowhead: EVs in MVBs. Scale: 1 µm. (**B**) P6/P56 iAT comparison of transcripts associated with endosomes, MVBs, lysosomes and exocytosis. (**C**) TEM image of EVs released by P6 adipocytes. Scale: 0.1µm. FACS analysis of nucleic acids in EVs of P6 adipocytes. N-St: non-stained; St: stained with SytoxGreen. Amount of EV-bound nucleic acids in cell culture media of P6 adipocytes. (**D**) Level of mtDNA in EVs of P6 adipocytes. *l:* light chain; *h:* heavy chain. (**E**) Labeling of dsRNA with J2 antibody in P6 adipocytes; scale: 10 µm. Quantification of RNA species released by EVs of P6 adipocytes. Effect of P6 EVs on mitochondrial content, mitobiogenesis (**F**), UCP1 level (**G**) and beige gene expression (**H**) in P56 adipocytes. -EVs: cells cultured in EV-free media, +EVs: cells treated with EVs. Scale: 10 µm (MTR); 50 µm (UCP1), MFI: mean fluorescence intensity. (**I**) Cytosolic delivery of mtDNA and mtRNA into 3T3-L1 cells, and their effect on beige gene transcription and mitobiogenesis. (**J**) Effect of P6 EVs on mitobiogenesis of adipocytes. *Ddx58*$^{-/-}$: RIG-I (DDX58)-deficient adipocytes, *Mda5*$^{-/-}$: MDA5-deficient adipocytes. **P*<0.05, ***P*<0.01, ****P*<0.001. Student's 2-tailed unpaired *t*-test or one-way ANOVA with Dunnett's post-hoc test. (**K**) Scheme of mtRNA-activated signal transduction in infant adipocytes.

Suppressed IRF7 signaling permits beige adipogenesis by mtRNA

P56 adipocytes expressed IRF7, unlike P6 adipocytes. Activation of the STING/AIM2 and RIG-I/MDA5 pathway was strong in P56 adipocytes with synthetic ligands, with mtRNA or with mtDNA, leading to *Ifnb* expression (Fig. S13A). Ultimately, IFNβ damaged adipocyte mitochondria (Fig. S13B,C). In turn, IRF7-deificient adipocytes were immune privileged for mitochondria (Fig. 3A, S4E), and mice lacking IRF7 retained their beige adipocytes to adulthood (Fig. 3B). This is coherent with the protection of IRF7-deficient mice from obesity (32). Moreover, P6 EVs reduced *Irf7* mRNA and IRF7 protein levels in adipocytes (Fig. 3C) and did not induce IFN-response (Fig. S13D). On the contrary, P56 EVs induced IFN-response and triggered *Irf7* expression, and reduced mitochondrial content in adipocytes (Fig. S13D,E).

Vitamin D receptor (VDR)-controlled gene networks were highly expressed in P6 iAT (Fig. S2A). The known VDR-target *Camp*, encoding cathelicidin, an adipose tissue enriched antimicrobial peptide (33), was highly expressed at P6. In turn, the VDR-repressed gene *Coro1a* had a low transcript level at P6 (Fig. 3D). *Coro1a* encodes coronin A1, also known as tryptophan-aspartate containing coat protein (TACO), which inhibits autophagosome formation (34). Low levels of coronin A1 allow autophagy (34), which is in accordance with the prominent autophagy we found in P6 iAT (Fig. 1H). The transcription of vitamin D metabolizing enzymes favored the storage of vitamin D3 (Vit-D3) and the synthesis of the potent VDR-agonist calcitriol in P6 iAT (Fig. 3D). Moreover, miR434-3p, a VDR-controlled miRNA which had complementarity to *Irf7* mRNA (35) was also highly expressed in P6 iAT (Fig. 3E). IRF7 level and inflammasome activation was effectively reduced by miR434-3p in adipocytes (Fig. 3E). Moreover, P6 EVs were rich in Vit-D3, and cytosolic mtRNA increased the transcription of the calcitriol synthesis gene *Cyp27b1* in adipocytes (Fig. 3F). VDR protein expression was higher in P6 than in P56 iAT, and

Vit-D3 effectively suppressed *Irf7* transcription in a VDR-dependent manner in adipocytes (Fig. 3F). Diet-induced obesity diminished adipocyte *Vdr* expression, and concomitantly upregulated *Irf7* in mice (Fig. 3G). Accordingly, inhibition of VDR signaling in young mice led to the loss of beige adipocytes in iAT, along with increased IRF7 level in adipocytes (Fig. 3H). In turn, suppression of IRF7 level with miR434-3p protected from inflammasome activation in adipocytes of HFD-fed mice (Fig. 3I).

IRF7 is a hub for the transcription of AIM2/STING pathway (Fig. 13F,G), and thus repression of IRF7 expression is a potential mechanism that protects infant adipocytes from an IFN-response to cytosolic mtDNA/mtRNA (Fig. 13H). We found that VDR signaling suppressed IRF7 expression and abolished immune response towards cytosolic mtDNA/mtRNA in mouse and human adipocytes (Fig. 3J-L), but did not affect *Il6* transcription and IL-6 release (Fig. 3K,L). VDR thus did not block the beige adipocyte-inducing IL-6 production, however suppressed IRF7-dependent inflammatory signaling. This allowed cytosolic mtRNA to induce mitobiogenesis and beige gene expression, and mtDNA to trigger mitophagy, without unfavorable induction of an IFN-response (Fig. 3M).

Obesity in early postnatal life compromises immune privilege of adipocyte mitochondria

We found that childhood obesity compromised VDR-controlled gene networks and decreased the expression of the calcitriol producing *CYP27A1* (Fig. 4A), and increased *IRF7* expression in the iAT (Fig. 1E). Similarly, diet induced obesity compromised *Vdr* and increased *Irf7* expression in mouse, and inhibition of VDR signaling in infant mice led to the loss of beige fat cells (Fig. 3G,H). Next, we studied a mouse model of childhood obesity, using infant mice which were nursed by dams fed with HFD (Fig. 4B) (36). In the offspring of HFD-fed dams adipocytes had a

compromised *Vdr*, and a robust *Irf7* expression (Fig. 4C), and beige adipocytes were lacking from the iAT (Fig. 4D). Eventually obesity developed and the adipocytes had a sustained inflammasome activation (Fig. 4E). Moreover, the mitochondrial network was compromised in adipocytes (Fig. 4F), and AIM2/STING pathway proteins were expressed in the cytosol and in the nuclei of adipocytes of mice nursed by HFD-fed dams (Fig. 4F). In turn, Vit-D3 reverted these adverse effects and protected the beige adipocyte content in infant mice (Fig. 4G), reduced obesity and adipocyte inflammation (Fig. 4H). In adult HFD-fed mice, cytosolic delivery of mtRNA into the iAT, combined with Vit-D3 treatment, reduced IRF7 level and increased beige adipocyte content in the iAT (Fig. 4I,J), reduced obesity and adipocyte inflammation, increased mitochondrial mass, thermogenesis and energy expenditure, inhibited inflammasome activation following STING activation, and induced adipocyte expression of calcitriol forming *Cyp27b1* (Fig. 4K-N, Fig. S14A-C).

Altogether, the immune privilege of mitochondrial content was dependent on the suppression of adipocyte IRF7 level by VDR. In human, childhood obesity compromised VDR signaling and increased *IRF7* expression in the adipose tissue. Adipocyte maturation increased IRF7 level, and in turn, Vit-D3 reduced IRF7 expression and immune response to cytosolic mtRNA and mtDNA in human adipocytes. Similarly, diet induced obesity compromised *Vdr* and triggered *Irf7* transcription in both adult and infant mice and triggered immune response against cytosolic mtDNA and mtRNA. These data show that beige adipocytes lack an immune response against mtDNA/mtRNA at least in part due to VDR signaling (Fig. 5A). When VDR sustains this immune privilege of mitochondria, cytosolic mtRNA stimulates the expression of nucleus-encoded mitochondrial genes and promotes beige adipocyte development (Fig. 5B). This mitochondria-to-nucleus signaling protects against obesity.

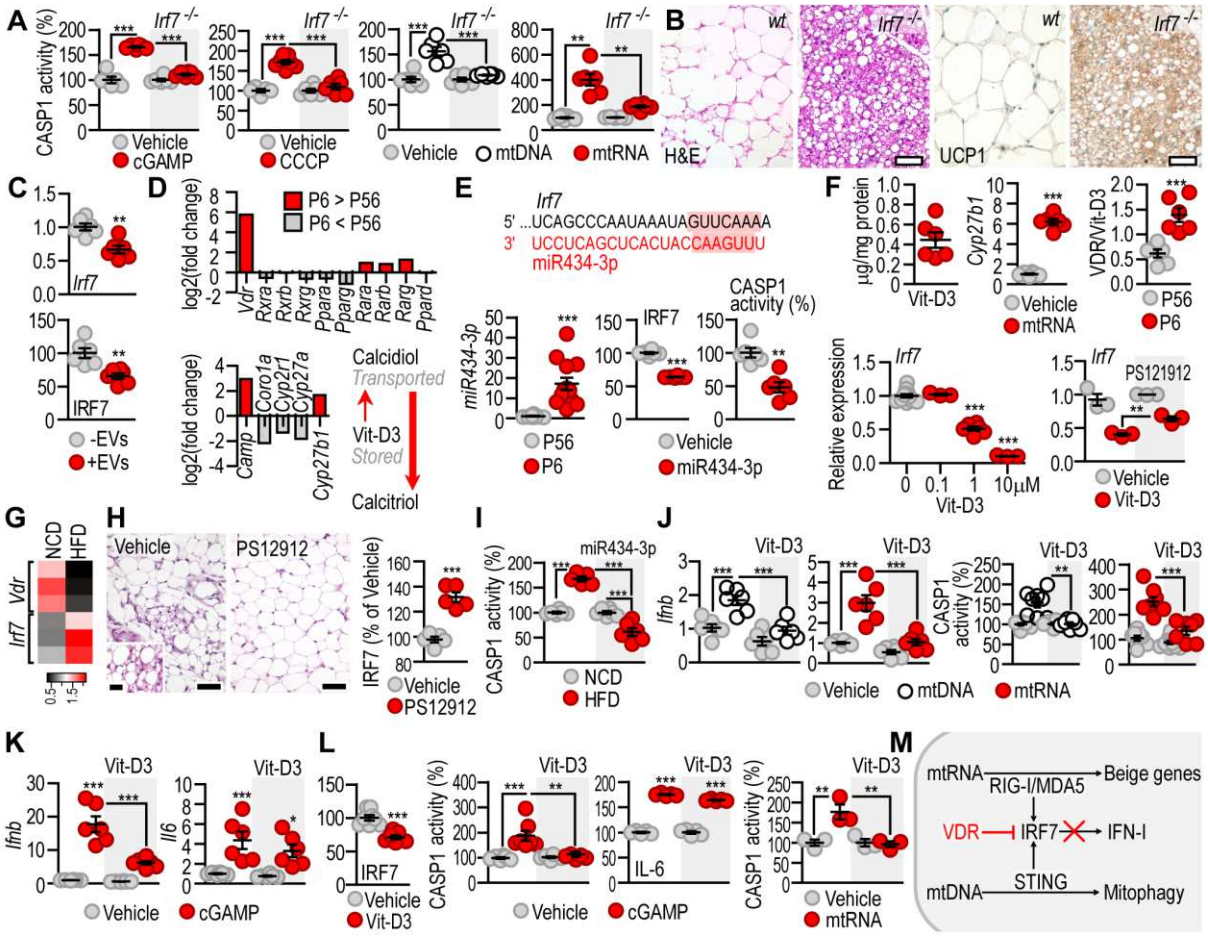

Fig. 3. VDR abrogates IRF7 expression in the infant adipocytes

(**A**) Response of P56 adipocytes to cGAMP, CCCP (carbonyl cyanide m-chlorophenyl hydrazone)-induced mitochondrial damage, cytosolic mtDNA and mtRNA. *Irf7*$^{-/-}$: IRF7-deficient adipocytes. (**B**) iAT of adult *wt* and *Irf7*$^{-/-}$ mice. Scale: 25 µm. H&E: hematoxylin-eosin (**C**) Effect or P6 EVs on *Irf7* and IRF7 level in mouse adipocytes (**D**) Structure of miR434-3p, its level in P6 and P56 iAT, and its effect on IRF7 level and inflammasome activity in mouse adipocytes. (**E**) P6/P56 transcript level of *Vdr,* VDR-controlled genes and vitamin D metabolism genes in iAT. (**F**) *Top:* Level of Vit-D3 in P6 EVs, effect of cytosolic mtRNA on the expression of calcitriol synthesizing *Cyp27b1*, and the ratio of VitD3/VDR in P6 iAT. *Bottom:* Effect of 48h Vit-D3 treatment on *Irf7* level in mouse adipocytes. PS121912: VDR inhibitor. (**G**) Level of *Vdr* and *Irf7* in iAT of HFD-fed mice. (**H**) *Left:* Histology of iAT at P10 of mice treated with vehicle or PS12912. Scale: 25 µm. *Right:* Adipocyte IRF7 protein level of the same mice. (**I**) Effect of overexpression of miR434-3p on HFD-induced inflammasome activation in adipocytes. (**J**,**K**) Response of 1 µM Vit-D3 pretreated mouse adipocytes to cytosolic mtDNA, mtRNA, or cGAMP. (**L**) IRF7 level and cGAMP response of human adipocytes treated with vehicle or Vit-D3. **P*<0.05, ***P*<0.01, ****P*<0.001. Student's 2-tailed unpaired *t*-test or one-way ANOVA with Dunnett's post-hoc test. (**M**) Scheme of VDR function in infant adipocytes.

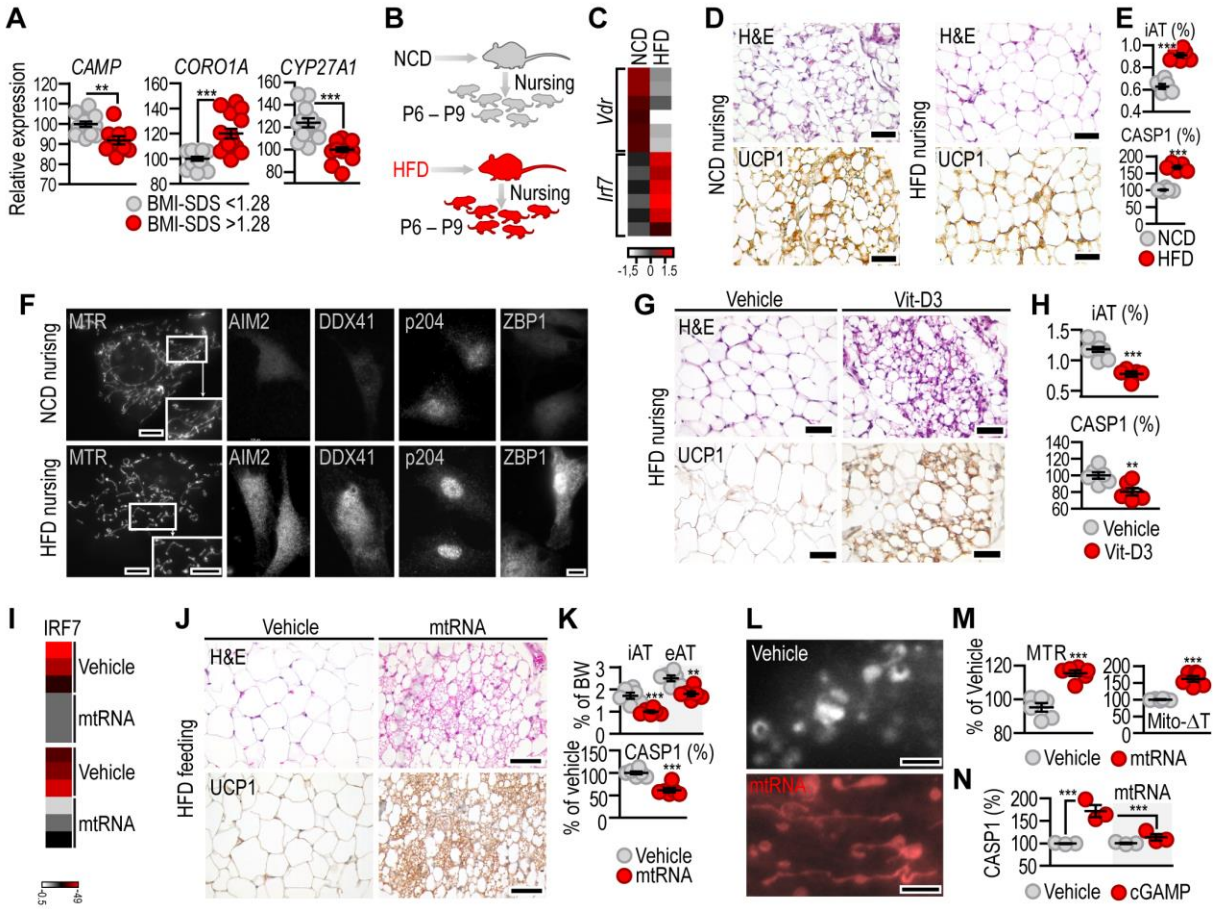

Fig. 4. Effect of cytosolic mtRNA combined vit Vit-D3 treatment in diet-induced obesity
(**A**) VDR-controlled gene expression in iAT of children. (**B**) Nursing mice received high-fat diet (HFD) or normal chow diet (NCD) between postnatal day 6 and 9 of the offspring. Mice nursed by NCD-fed or HFD-fed dams were analyzed on postnatal day 10 (P10). (**C**) *Vdr* and *Irf7* expression in iAT. (**D**) Histology of iAT. H&E: hematoxylin and eosin staining, UCP1: UCP1 immunostaining, Scale: 50 μm. Note the lack of multilocular adipocytes in mice nursed by HFD-fed dams. (**E**) Ratio of iAT and body weight, and inflammasome caspase 1 (CASP1) activity of the adipocytes. (**F**) Mitochondrial network and the expression of AIM2, DDX41, p204 and ZBP1 in adipocytes. MTR: MitoTracker Red. Scale 50 μm. (**G**) Mice were nursed by HFD-fed dams, and treated with vehicle or Vit-D3 from P6 to P9. Histology of iAT on P10. Scale: 100 μm (**H**) Ratio of iAT and body weight, and CASP1 activity of the adipocytes on P10. (**I**) In adult HFD-fed mice the iAT was transfected with vehicle or mtRNA, and IRF7 protein level was measured in adipocytes. (**J**) Histology of iAT of vehicle- or mtRNA-transfected mice. (**K**) Adipose tissue weight/body weight ratio, and CASP1 activity of adipocytes. eAT: epididymal adipose tissue (**L**) Mitochondrial network of adipocytes isolated from vehicle- or mtRNA-transfected mice. Scale: 10 μm. Note the expansion of the mitochondrial network after mtRNA treatment. (**M**) Mitochondrial mass (relative MTR fluorescent intensity) and mitochondrial temperature change (Mito-ΔT) in adipocytes isolated from vehicle- or mtRNA-transfected mice. (**L**) CASP1 activity of adipocytes isolated from vehicle- or mtRNA-transfected mice, and treated with vehicle of cGAMP for 4h. ***P*<0.01, ****P*<0.001. Student's 2-tailed unpaired *t*-test or one-way ANOVA with Dunnett's post-hoc test.

Discussion

Adipose tissue inflammation is considered deleterious for metabolism (37). However, various lines of evidence show that differentiation of thermogenic adipose tissue requires JAK/STAT3 signaling (7, 38, 39), and an autocrine IL-6/STAT3 signaling loop is sustained by breast milk-derived lipid signaling in the newborn adipose tissue (7). Some inflammatory signal mechanisms that cause obesity-associated metabolic impairment also sustain beige adipocytes (40, 41). Here we report the unexpected finding that beige adipocyte development is promoted by a potentially inflammation-evoking cytosolic RNA signal, released by the mitochondria of infant adipocytes.

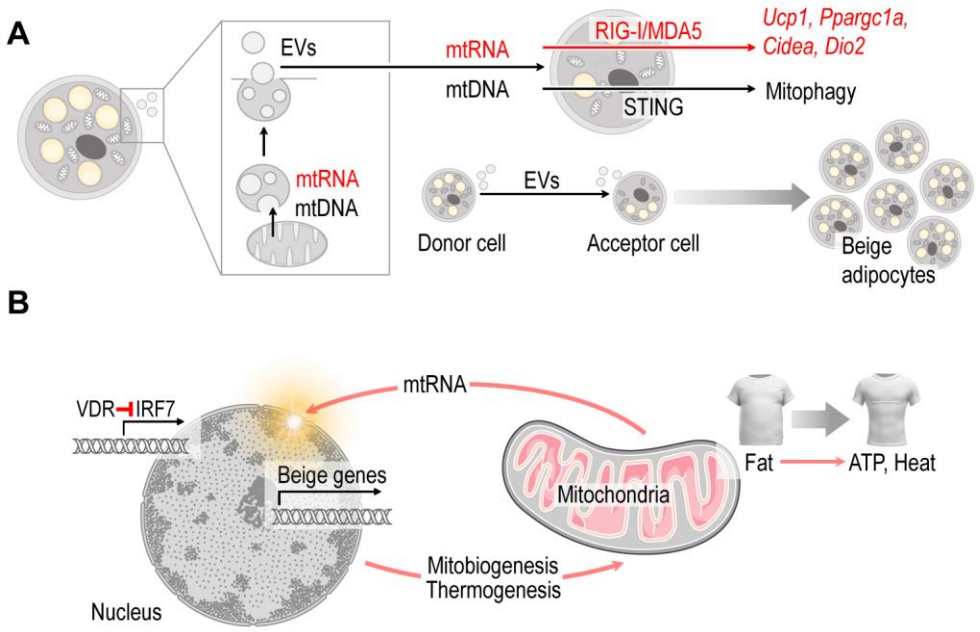

Fig. 5. Role of mtRNA signaling in beige adipocytes
(A) Under physiological conditions infant adipocytes release cytosolic mtRNA and mtDNA in extracellular vesicles (EVs). Eventually, mtRNA serves as endogenous signal for beige adipogenesis in neighboring cells through the RIG-I/MDA5/IL-6/STAT3 pathway. In turn, mtDNA content of the EVs triggers mitophagy through STING signaling. (**B**) Albeit cytosolic mtRNA and mtRNA are noxious signals, they can act as metabolically beneficial mitochondria-to-nucleus signals when IRF7 expression is suppressed. VDR is an effective suppressor of IRF7 and abrogates IFN-response to cytosolic mtRNA and mtDNA in infant adipocytes. Infant adipocytes are hence immune privileged sites for mitochondria, allowing a retrograde mitochondria-to-nucleus signaling through mtRNA, which is key for mitobiogenesis and beige fat development.

The endosymbiotic origin of mitochondria has led to a metabolic co-dependence of the mitochondria and the host cell (42). This is driven by a retrograde, mitochondria-to-nucleus signaling pathway, as the majority of genes required for the maintenance of mitochondria are encoded in the nuclear genome. We show that, analogous to a parasite-host interaction, mitochondrial nucleic acids are released by EVs, and are taken up by surrounding adipocytes to activate cytosolic RNA sensors that stimulate an autocrine IL-6/STAT3 signaling loop, ultimately triggering the nuclear expression of beige adipocyte genes (Fig. 2K, Fig. 5A). Non-coding RNA species of mitochondria are known to increase the transcription of mitochondrial genome-encoded genes (27). As an equivalent mechanism, we show that mtRNA species boost the transcription of nuclear genome-encoded genes for mitochondrial biogenesis and thermogenesis. This is key for mitobiogenesis since the majority of the mitochondrial genes are encoded in the nuclear genome (42). The release of EVs containing mitochondrial nucleic acids resembles the recently explored mechanism that allows nucleic acid delivery from bacteria to host cells in membrane microvesicles (43, 44).

The primary sensors of cytoplasmic mtRNA are RIG-I and MDA5. RIG-I detects dsRNAs with or without a 5′-triphosphate end; MDA5 binds uncapped RNA; and RIG-I and MDA5 selectively recognize short and long dsRNAs, respectively (29, 30). Given the prokaryote origin of mitochondria, various mtRNA species such as mitochondrial ribosomal RNAs, uncapped mitochondrial mRNA, and non-coding mtRNAs, can potentially stimulate the cytoplasmic RNA sensor system (45, 46). Beige adipocyte gene transcription was achievable by indirect RIG-I activation using cytosolic p(dA:dT), and also by MDA5 activation using cytosolic high molecular weight p(I:C), but not with cytosolic ssRNA. Coherently, lack of RIG-I and MDA5 signaling

compromised the mtRNA-mediated beige adipocyte development, and abrogated nucleus-encoded SDH-A expression and mitobiogenesis, and promoted the loss of beige adipocytes in mice.

Nevertheless, excessive release of mitochondrial content is a danger signal, and activates an IFN-response, which is detrimental for thermogenic fat development (16, 47, 48), triggers obesity, mitochondrial dysfunction and the mitochondrial pathway of adipocyte apoptosis (49, 50), and may aggravate obesity-associated metabolic diseases (51, 52). We show here that beige adipocytes lack cytosolic DNA sensors and show suppressed expression of IRF7. Consequently, cytosolic mtDNA and mtRNA do not stimulate an IFN-response in beige adipocytes. Instead, beige adipocytes respond by activating mitophagy to cytoplasmic mtDNA, allowing the removal of damaged mitochondria and curtailing inflammation. Moreover, cytosolic mtRNA stimulates mitobiogenesis. The key protective mechanism – i.e., compromised IRF7 signaling – is a trait of the infant adipocytes, and is lost in the course of adipocyte maturation. While the activation of STAT1 and NFκB signaling may account for the increasing IRF7 expression during adipocyte maturation (6), we show that VDR signaling contributes to the suppression of IRF7 level in infant adipocytes, and cytosolic mtRNA stimulates mitochondrial calcitriol synthesis – hence supplies a VDR ligand – in infant adipocytes. However, diet-induced obesity in mouse, and obesity in children were associated with robust expression of the cytosolic DNA sensor system and IRF7, leading to the loss of the immune privilege of mitochondria.

VDR signaling is involved in the innate immune response in the adipose tissue (33), and VDR may also skew IFN-response and IRF7 expression (53, 54). Vit-D3 supplementation is today routine in postnatal care, however, Vit-D3 deficiency is prevalent among obese children and adolescents and is a risk factor for metabolic diseases (55-57). Vit-D3/VDR is proposed to inhibit weight gain by activating UCP3 in the muscles (58), albeit VDR overexpression promotes weight

292 gain in mouse (59). Indeed, promotion of formula feeding originally served to increase Vit-D3
293 supply and induce weight gain (60). Formula milk lacks maternal lipid species that maintain beige
294 fat and has obesogenic effects (7). We also show here that formula milk lacks beige-inducing
295 mtRNA signals. Moreover, VDR signaling was impaired in the adipose tissue of obese children,
296 therefore despite its increased Vit-D3 level, formula milk is not sufficient to trigger beige
297 adipogenesis. However, when Vit-D3 supplementation is combined with stimulation of cytosolic
298 mtRNA signaling, beige adipocytes develop and obesity is reduced.

299 In summary, beige adipocyte development is dependent on a mtRNA-mediated signaling
300 and the suppression of IFN-response. Restoring the mtRNA-mediated mitochondria-to-nucleus
301 signaling may represent a novel and effective mechanism to increase beige fat and reduce obesity.

Methods

Animals and cells

We used *wt* male C57BL/6 (Charles River Laboratories, Wilmington, MA), *Irf7*$^{-/-}$ (RIKEN, Wako, Japan), *Ddx58*$^{-/-}$ and *Mda5*$^{-/-}$ (kindly provided by Gunther Hartmann, University of Bonn, Germany) mice. All mouse lines were housed under SPF conditions. Animal experiments were approved by the local ethics committees. Primary mouse adipocytes were isolated by collagenase digestion and separation of cell fractions and subsequently analyzed or cultured, as described (7).

Human samples

Subcutaneous adipose tissue from human infants, adolescents and young adults were collected in the Leipzig Childhood Adipose Tissue cohort during elective surgery (3). For all children included in the study written informed consent was obtained from the parents. The study protocol was approved by the local ethics committee of the Medical Faculty, University of Leipzig (#265-08-ff; NCT02208141). Adult adipocytes samples were collected in our previous study (7).

mRNA analysis and next-generation sequencing

Extraction of total RNA was performed as described (6). qPCR assays were carried out on the Quantabio platform (Beverly, MA), using *Bactin*, *Gapdh* and *Ppia* as references. Primer sequences are provided in Supplemental Table 1. NGS analysis was carried out on the BGISEQ-500 platform by BGI Genomics Inc. (Cambridge, MA), generating about 26.20M reads per sample (Fig. S15). EnrichR, Panther and Interferome-2.0 were used for annotation of transcripts; clustered image maps (CIMs, heat-maps) were rendered by CIM-Miner and Heatmapper. Gene expression in human samples was quantified by ILLUMINA HT12v4 Gene Expression BeadChip arrays and data were background corrected and quantile normalized (6).

Supplemental methods

Cytosolic delivery of RNA/DNA, viral infections, ELISA assays, overexpression studies, autophagosome/lysosome labeling, EV collection, FACS, histology, image analysis, and TEM analysis are provided in the Supplemental Information.

Data representation and statistics

Data are represented as mean±s.e.m, along with each individual data point. When data are represented as CIMs to visualize gene transcription differences between experimental conditions, we indicate fold changes or Z-scores of the relative abundance. Statistical significance is indicated as $*P<0.01$, $**P<0.01$; $***P<0.001$, Student's 2-tailed unpaired *t*-test, or 1-way ANOVA with Dunnett's post hoc test.

Data and materials availability

Materials and data are available for secondary use upon request. Flow Repository identifiers of FACS data are as follows: #FR-FCM-Z236, #FR-FCM-Z2R6, #FR-FCM-ZYPU, #FR-FCM-ZYUU. NGS data are deposited at GEO with the accession number #GSE185317. For secondary analysis, we used our previously published DNA Chip and NGS datasets, with accession numbers #GSE125405, #GSE90658, #GSE154925 and #GSE133500.

Acknowledgements

We thank Dr. Kenneth McCreath for editing the manuscript.

Funding

This study was supported by the German Research Fund (DFG, RO 4856-1, to TR; DFG, CRC1052 C05, to AK), the European Foundation for the Study of Diabetes on New Targets for Type 2 Diabetes, Supported by MSD (No. 96403, to TR), by the Federal Ministry of Education and Research (BMBF), Germany (FKZ: 01EO1501 IFB Adiposity Diseases, to AK.

Author contribution

ACH, HY, YTL, CCC, VD carried out experiments, AK, AH, JC designed experiments, TR conceived the project, designed experiments and wrote the manuscript.

References

1. Chobot A, Górowska-Kowolik K, Sokołowska M, and Jarosz-Chobot P. Obesity and diabetes—Not only a simple link between two epidemics. *Diabetes/Metabolism Research and Reviews.* 2018:e3042.
2. Geserick M, Vogel M, Gausche R, Lipek T, Spielau U, Keller E, et al. Acceleration of BMI in early childhood and risk of sustained obesity. *The New England journal of medicine.* 2018;379(14):1303-12.
3. Landgraf K, Rockstroh D, Wagner IV, Weise S, Tauscher R, Schwartze JT, et al. Evidence of early alterations in adipose tissue biology and function and its association with obesity-related inflammation and insulin resistance in children. *Diabetes.* 2015;64(4):1249-61.
4. Herrera E, and Amusquivar E. Lipid metabolism in the fetus and the newborn. *Diabetes Metab Res Rev.* 2000;16(3):202-10.
5. Stave U. *Perinatal physiology.* New York, London: Plenum Medical Company; 1970.
6. Hoang AC, Yu H, and Röszer T. Transcriptional Landscaping Identifies a Beige Adipocyte Depot in the Newborn Mouse. *Cells.* 2021;10(9):2368.
7. Yu H, Dilbaz S, Coßmann J, Hoang AC, Diedrich V, Herwig A, et al. Breast milk alkylglycerols sustain beige adipocytes through adipose tissue macrophages. *The Journal of Clinical Investigation.* 2019;129(6):2485-99.
8. Ikeda K, Maretich P, and Kajimura S. The Common and Distinct Features of Brown and Beige Adipocytes. *Trends in Endocrinology & Metabolism.* 2018;29(3):191-200.
9. Hahn P, and Novak M. Development of brown and white adipose tissue. *Journal of lipid research.* 1975;16(2):79-91.

10. Rockstroh D, Landgraf K, Wagner IV, Gesing J, Tauscher R, Lakowa N, et al. Direct evidence of brown adipocytes in different fat depots in children. *PLOS ONE.* 2015;10(2):e0117841.
11. Zhong Z, Liang S, Sanchez-Lopez E, He F, Shalapour S, Lin XJ, et al. New mitochondrial DNA synthesis enables NLRP3 inflammasome activation. *Nature.* 2018;560(7717):198-203.
12. Beyerlein A, Donnachie E, Jergens S, and Ziegler A-G. Infections in Early Life and Development of Type 1 Diabetes. *JAMA.* 2016;315(17):1899-901.
13. Atkinson RL. Viruses as an etiology of obesity. *Mayo Clinic proceedings.* 2007;82(10):1192-8.
14. Shoelson SE, Lee J, and Goldfine AB. Inflammation and insulin resistance. *J Clin Invest.* 2006;116(7):1793-801.
15. Lempainen J, Tauriainen S, Vaarala O, Makela M, Honkanen H, Marttila J, et al. Interaction of enterovirus infection and cow's milk-based formula nutrition in type 1 diabetes-associated autoimmunity. *Diabetes Metab Res Rev.* 2012;28(2):177-85.
16. Kissig M, Ishibashi J, Harms MJ, Lim H-W, Stine RR, Won K-J, et al. PRDM16 represses the type I interferon response in adipocytes to promote mitochondrial and thermogenic programing. *The EMBO Journal.* 2017;36(11):1528-42.
17. Motwani M, Pesiridis S, and Fitzgerald KA. DNA sensing by the cGAS–STING pathway in health and disease. *Nature Reviews Genetics.* 2019;20(11):657-74.
18. Shin S-I, Ham S, Park J, Seo SH, Lim CH, Jeon H, et al. Z-DNA-forming sites identified by ChIP-Seq are associated with actively transcribed regions in the human genome. *DNA Res.* 2016;23(5):477-86.
19. Takaoka A, Wang Z, Choi M, Yanai H, Negishi H, Ban T, et al. DAI (DLM-1/ZBP1) is a cytosolic DNA sensor and an activator of innate immune response. *Nature.* 2007;448:501-5.
20. Lugrin J, and Martinon F. The AIM2 inflammasome: Sensor of pathogens and cellular perturbations. *Immunological Reviews.* 2018;281(1):99-114.
21. Geserick M, Vogel M, Gausche R, Lipek T, Spielau U, Keller E, et al. Acceleration of BMI in Early Childhood and Risk of Sustained Obesity. *The New England journal of medicine.* 2018;379(14):1303-12.

22. Bahat A, MacVicar T, and Langer T. Metabolism and Innate Immunity Meet at the Mitochondria. *Frontiers in Cell and Developmental Biology.* 2021;9(2019).
23. Liu D, Wu H, Wang C, Li Y, Tian H, Siraj S, et al. STING directly activates autophagy to tune the innate immune response. *Cell Death & Differentiation.* 2019;26(9):1735-49.
24. Devi TS, Yumnamcha T, Yao F, Somayajulu M, Kowluru RA, and Singh LP. TXNIP mediates high glucose-induced mitophagic flux and lysosome enlargement in human retinal pigment epithelial cells. *Biology open.* 2019;8(4):bio038521.
25. Nakahira K, Haspel JA, Rathinam VAK, Lee S-J, Dolinay T, Lam HC, et al. Autophagy proteins regulate innate immune responses by inhibiting the release of mitochondrial DNA mediated by the NALP3 inflammasome. *Nature immunology.* 2011;12(3):222-30.
26. Fujiwara Y, Wada K, and Kabuta T. Lysosomal degradation of intracellular nucleic acids—multiple autophagic pathways. *The Journal of Biochemistry.* 2016;161(2):145-54.
27. Ro S, Ma H-Y, Park C, Ortogero N, Song R, Hennig GW, et al. The mitochondrial genome encodes abundant small noncoding RNAs. *Cell Research.* 2013;23(6):759-74.
28. Rackham O, Shearwood A-MJ, Mercer TR, Davies SMK, Mattick JS, and Filipovska A. Long noncoding RNAs are generated from the mitochondrial genome and regulated by nuclear-encoded proteins. *RNA.* 2011;17(12):2085-93.
29. Dias Junior AG, Sampaio NG, and Rehwinkel J. A Balancing Act: MDA5 in Antiviral Immunity and Autoinflammation. *Trends in Microbiology.* 2019;27(1):75-85.
30. Kato H, Takeuchi O, Mikamo-Satoh E, Hirai R, Kawai T, Matsushita K, et al. Length-dependent recognition of double-stranded ribonucleic acids by retinoic acid-inducible gene-I and melanoma differentiation-associated gene 5. *The Journal of experimental medicine.* 2008;205(7):1601-10.
31. Abels ER, and Breakefield XO. Introduction to Extracellular Vesicles: Biogenesis, RNA Cargo Selection, Content, Release, and Uptake. *Cell Mol Neurobiol.* 2016;36(3):301-12.
32. Wang XA, Zhang R, Zhang S, Deng S, Jiang D, Zhong J, et al. Interferon regulatory factor 7 deficiency prevents diet-induced obesity and insulin resistance. *American journal of physiology Endocrinology and metabolism.* 2013;305(4):E485-95.
33. Zhang LJ, Guerrero-Juarez CF, Hata T, Bapat SP, Ramos R, Plikus MV, et al. Innate immunity. Dermal adipocytes protect against invasive Staphylococcus aureus skin infection. *Science.* 2015;347(6217):67-71.

34. Seto S, Tsujimura K, and Koide Y. Coronin-1a inhibits autophagosome formation around Mycobacterium tuberculosis-containing phagosomes and assists mycobacterial survival in macrophages. *Cellular Microbiology.* 2012;14(5):710-27.
35. Yu P, Song H, Gao J, Li B, Liu Y, and Wang Y. Vitamin D (1,25-(OH)2D3) regulates the gene expression through competing endogenous RNAs networks in high glucose-treated endothelial progenitor cells. *The Journal of Steroid Biochemistry and Molecular Biology.* 2019;193:105425.
36. Masuyama H, and Hiramatsu Y. Additive Effects of Maternal High Fat Diet during Lactation on Mouse Offspring. *PLOS ONE.* 2014;9(3):e92805.
37. Christ A, and Latz E. The Western lifestyle has lasting effects on metaflammation. *Nature Reviews Immunology.* 2019;19(5):267-8.
38. Derecka M, Gornicka A, Koralov SB, Szczepanek K, Morgan M, Raje V, et al. Tyk2 and Stat3 regulate brown adipose tissue differentiation and obesity. *Cell metabolism.* 2012;16(6):814-24.
39. Babaei R, Schuster M, Meln I, Lerch S, Ghandour RA, Pisani DF, et al. Jak-TGFβ cross-talk links transient adipose tissue inflammation to beige adipogenesis. *Science Signaling.* 2018;11(527).
40. Alsaggar M, Mills M, and Liu D. Interferon beta overexpression attenuates adipose tissue inflammation and high-fat diet-induced obesity and maintains glucose homeostasis. *Gene Ther.* 2017;24(1):60-6.
41. Cao W, Daniel KW, Robidoux J, Puigserver P, Medvedev AV, Bai X, et al. p38 Mitogen-Activated Protein Kinase Is the Central Regulator of Cyclic AMP-Dependent Transcription of the Brown Fat Uncoupling Protein 1 Gene. *Molecular and Cellular Biology.* 2004;24(7):3057-67.
42. Youle RJ. Mitochondria—Striking a balance between host and endosymbiont. *Science.* 2019;365(6454):eaaw9855.
43. Toyofuku M, Nomura N, and Eberl L. Types and origins of bacterial membrane vesicles. *Nature Reviews Microbiology.* 2019;17(1):13-24.
44. Bitto NJ, Chapman R, Pidot S, Costin A, Lo C, Choi J, et al. Bacterial membrane vesicles transport their DNA cargo into host cells. *Scientific reports.* 2017;7(1):7072-.

45. Eberle F, Sirin M, Binder M, and Dalpke AH. Bacterial RNA is recognized by different sets of immunoreceptors. *European Journal of Immunology.* 2009;39(9):2537-47.
46. Eigenbrod T, and Dalpke AH. Bacterial RNA: An Underestimated Stimulus for Innate Immune Responses. *The Journal of Immunology.* 2015;195(2):411-8.
47. Kumari M, Wang X, Lantier L, Lyubetskaya A, Eguchi J, Kang S, et al. IRF3 promotes adipose inflammation and insulin resistance and represses browning. *J Clin Invest.* 2016;126(8):2839-54.
48. Bai J, Cervantes C, He S, He J, Plasko GR, Wen J, et al. Mitochondrial stress-activated cGAS-STING pathway inhibits thermogenic program and contributes to overnutrition-induced obesity in mice. *Communications Biology.* 2020;3(1):257.
49. Bai J, and Liu F. The cGAS-cGAMP-STING Pathway: A Molecular Link Between Immunity and Metabolism. *Diabetes.* 2019;68(6):1099-108.
50. Gkirtzimanaki K, Kabrani E, Nikoleri D, Polyzos A, Blanas A, Sidiropoulos P, et al. IFNα Impairs Autophagic Degradation of mtDNA Promoting Autoreactivity of SLE Monocytes in a STING-Dependent Fashion. *Cell reports.* 2018;25(4):921-33.e5.
51. Tian Y, Jennings J, Gong Y, and Sang Y. Viral Infections and Interferons in the Development of Obesity. *Biomolecules.* 2019;9(11).
52. Birk RZ, and Rubinstein M. IFN-alpha induces apoptosis of adipose tissue cells. *Biochem Biophys Res Commun.* 2006;345(2):669-74.
53. Cippitelli M, and Santoni A. Vitamin D3: a transcriptional modulator of the interferon-γ gene. *European Journal of Immunology.* 1998;28(10):3017-30.
54. Stoppelenburg AJ, von Hegedus JH, Huis in't Veld R, Bont L, and Boes M. Defective control of vitamin D receptor-mediated epithelial STAT1 signalling predisposes to severe respiratory syncytial virus bronchiolitis. *The Journal of Pathology.* 2014;232(1):57-64.
55. Roth CL, Elfers C, Kratz M, and Hoofnagle AN. Vitamin d deficiency in obese children and its relationship to insulin resistance and adipokines. *J Obes.* 2011;2011:495101-.
56. de Oliveira LF, de Azevedo LG, da Mota Santana J, de Sales LPC, and Pereira-Santos M. Obesity and overweight decreases the effect of vitamin D supplementation in adults: systematic review and meta-analysis of randomized controlled trials. 2020;21(1):67-76.
57. Pramono A, Jocken JWE, and Blaak EE. Vitamin D deficiency in the aetiology of obesity-related insulin resistance. 2019;35(5):e3146.

58. Fan Y, Futawaka K, Koyama R, Fukuda Y, Hayashi M, Imamoto M, et al. Vitamin D3/VDR resists diet-induced obesity by modulating UCP3 expression in muscles. *J Biomed Sci.* 2016;23(1):56-.
59. Xu Y, Lou Y, and Kong J. VDR regulates energy metabolism by modulating remodeling in adipose tissue. *European journal of pharmacology.* 2019;865:172761.
60. Biggs K, Hurrell K, Matthews E, Khaleva E, Munblit D, and Boyle R. Formula Milk Supplementation on the Postnatal Ward: A Cross-Sectional Analytical Study. *Nutrients.* 2018;10(5):608.

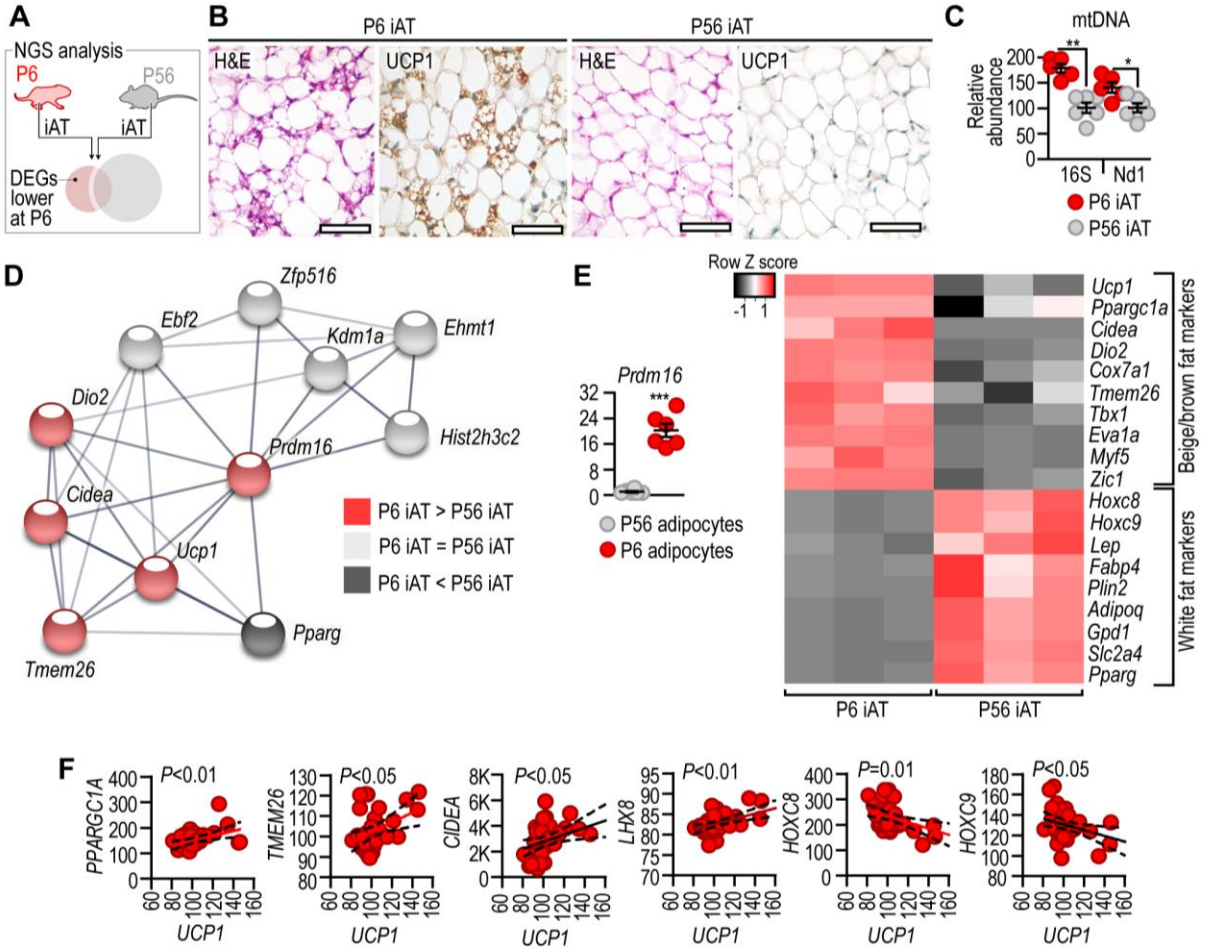

Supplemental Figure 1. Characterization of mouse inguinal adipose tissue at P6 and P56, and human inguinal adipose tissue in infancy

(**A**) Scheme of NGS analysis. For RNA sequencing we obtained inguinal fat depots (iAT) of 3-3 mice at postnatal day 6 (P6) and P56 and compared their transcriptional profiles. The differentially expressed genes (DEGs) were analyzed further in this study. (**B**) Hematoxylin and eosin (H&E) staining, and immunostaining of UCP1 in mouse iAT at P6 and P56. Scale: 50 μm. (**C**) Abundance of mtDNA (*16S* and *Nd1* genes) relative to genomic DNA in mouse iAT at P6 and P56. (**D**) Gene network associated with PR/SET domain 16 (PRDM16), a key regulator of brown adipocyte development (1-3). Red symbols indicate DEGs overrepresented in P6 iAT. Beige/brown adipocyte-associated genes were overrepresented in P6 iAT. (**E**) Transcription of *Prdm16* in mouse adipocytes at P6 and P56. Heat map summarizing the transcription level of beige/brown adipocyte marker genes and white adipocyte marker genes in P6 and P56 iAT. *Ucp1* is necessary for thermogenesis; *Ppargc1a* for mitochondrial biogenesis; *Cidea*, *Cox7a1, Dio2, Zic1* are associated with brown/beige adipocytes; *Tmem26* and *Tbx1* are beige adipocyte markers; *Eva1a* is a brown adipocyte marker (4-9); *Myf5* is expressed by progenitors of brown adipocytes (10). Levels of *Hoxc8* and *Hoxc9* increase along white adipocyte development (4), although *Hoxc9* may also be a marker of beige adipocytes (9). *Lep*, *Fabp4*, *Plin2*, *Adipoq*, *Gpd1*, *Slc2a4* and *Pparg* are associated with white adipocyte maturation (11). See also (12). (**F**) Correlation of *UCP1* levels with beige/brown adipocyte-associated transcripts (*PPARGC1A*, *TMEM26*, *CIDEA*, *LHX8*) and white adipocyte markers (*HOXC8*, *HOXC9*) in the iAT of human male infants (4, 13). *P* values were determined with linear regression analysis. Age 0.2–3.5 years. Further details regarding beige adipocyte content in mouse and human fat depots are provided in (4, 12-14), and reviewed in the introduction section of (3).

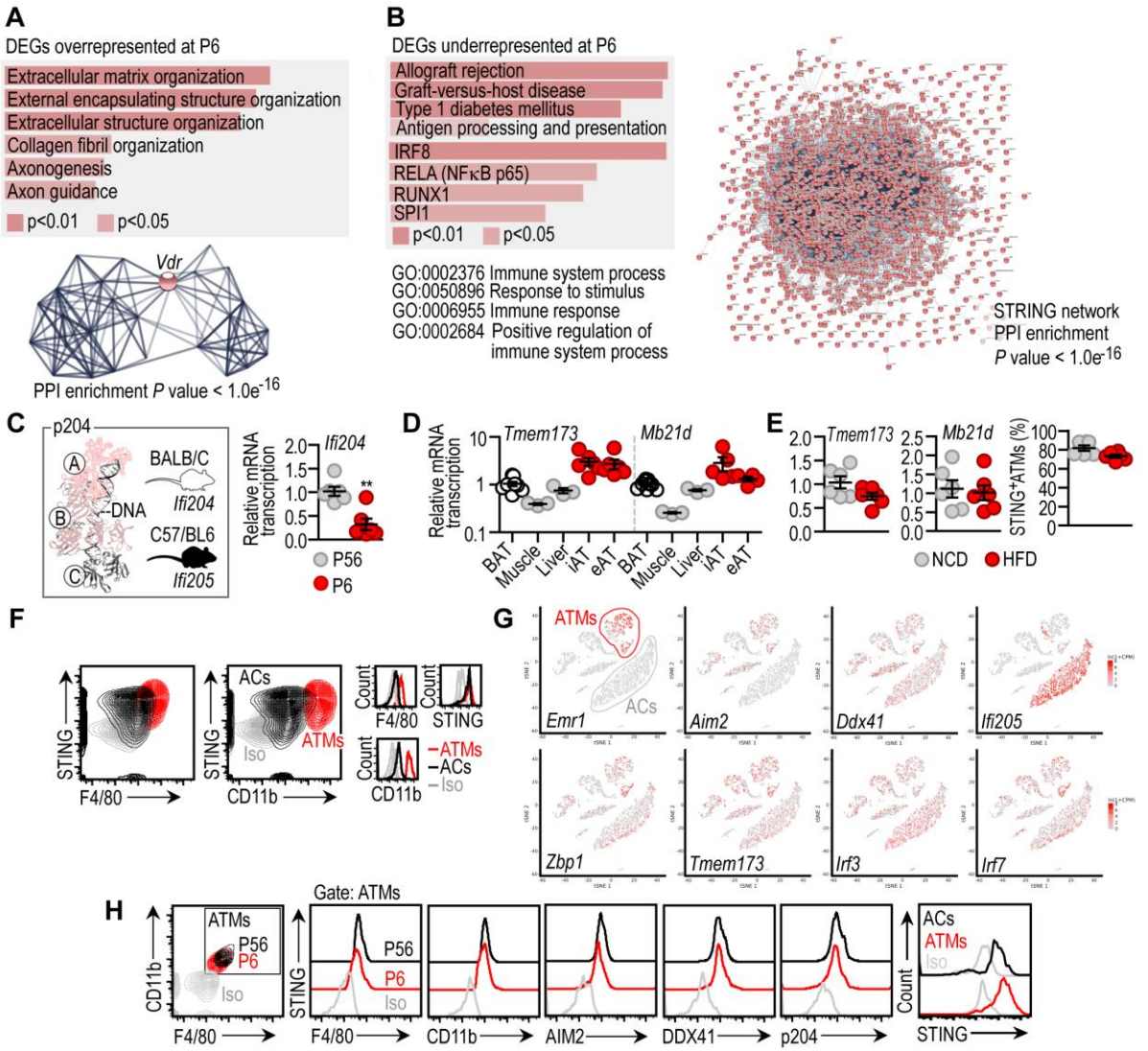

Supplemental Figure 2. Expression of the STING/AIM2 pathways in P6 and P56 iAT

(**A**) Gene ontology and STRING protein-protein association network of DEGs overrepresented in P6 iAT. Further analysis is available in (12). *Vdr* and its gene network were overrepresented at P6. (**B**) Gene ontology and protein-protein association network of underrepresented DEGs at P6 (15). (**C**) Structure of the DNA-sensor p204. The three DNA-binding domains are labeled A, B and C. p204 is encoded by *Ifi204* in BALB/C mice. In C57/BL6, however, *Ifi204* has a frameshift mutation and its function is taken over by *Ifi205* (16-18). In 3T3-L1 cells, which have a BALB/C origin, we measured *Ifi204*, whereas we measured *Ifi205* in adipocytes from C57/BL6 mice. Level of *Ifi204* in P6 and P56-derived adipocytes mirrored that of *Ifi205*, shown in Figure 1. (**D**) Expression of *Tmem173* and *Mb21d* in metabolic organs at P56. Note their prominent expression in iAT and in the epididymal adipose tissue (eAT). (**E**) Level of *Tmem173* and *Mb21d* in iAT of mice fed normal chow diet (NCD) or high-fat diet (HFD). Amount of STING-expressing ATMs in iAT following NCD or HFD. STING expression was not influenced by HFD. (**F**) FACS plot of adipose tissue macrophages (ATMs) and adipocytes (ACs) from iAT. ATMs were defined as F4/80$^+$, CD11b$^+$. (**G**) Single cell sequencing data retrieved from the TabulaMuris consortium (19), showing that the STING pathway is expressed in both ATMs and in adipocytes. There is a marked expression of *Ifi205* in adipocytes. (**H**) FACS analysis of the STING pathway in ATMs at P6 and P56.

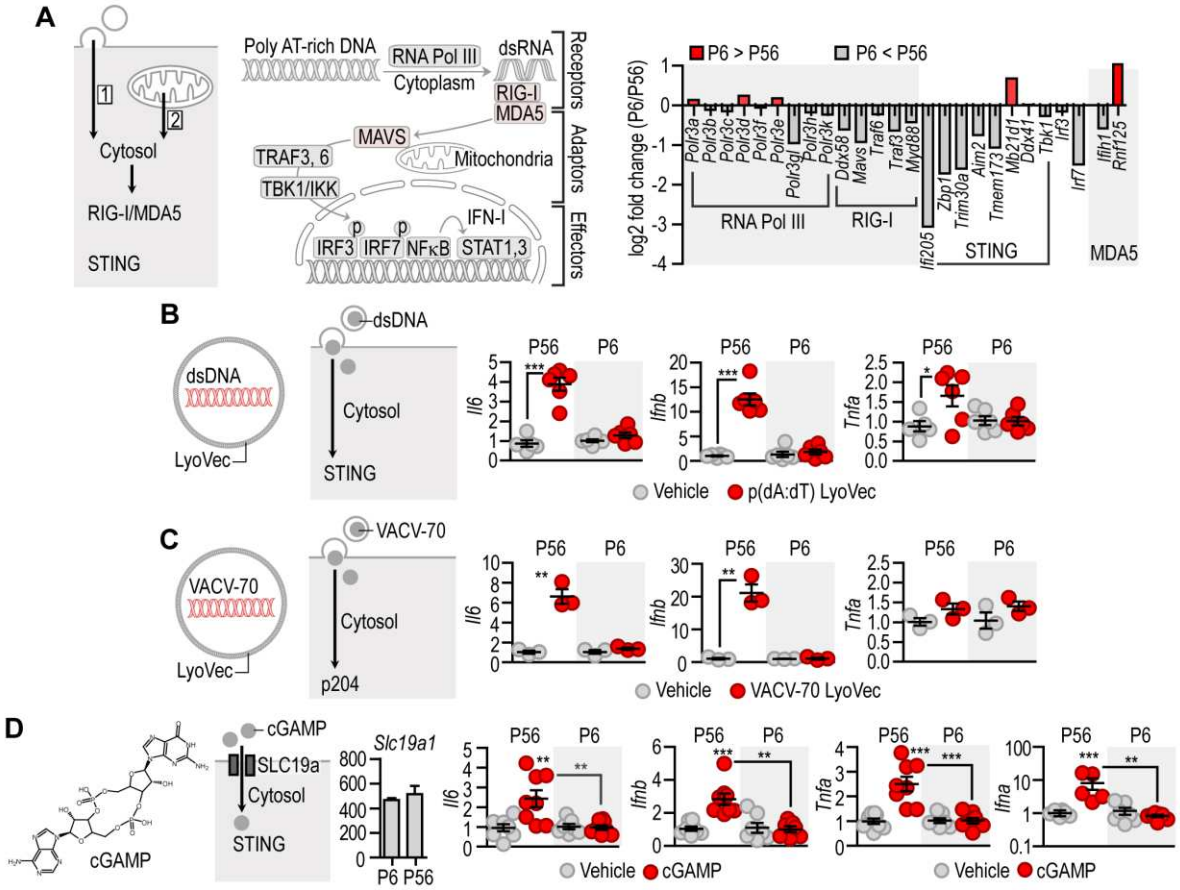

Supplemental Figure 3. Cytosolic DNA sensing in adipocytes

(**A**) *Left:* Possible routes of DNA and RNA release into the cytosol: membrane fusion with EVs [**1**]; release of mtDNA and mtRNA into the cytosol [**2**]. Both mechanisms can activate RIG-I/MDA5 or STING signaling. *Middle:* Scheme of RIG-I/MDA5 signaling. RNA Pol III: RNA polymerase III, which can generate dsRNA from DNA templates, ultimately activating the RIG-I/MDA5 pathway. *Right:* Expression of RNA Pol III and RIG-I/MDA5 pathway genes in P6 iAT. As a comparison, genes of the STING signaling pathway are also shown. See also the heatmap in Figure 1. (**B**) *Left:* Scheme of LyoVec-encapsulated dsDNA. The LyoVec lipid carrier fuses with the cell membrane and dsDNA is released into the cytosol of the recipient cell. *Right:* Responsiveness of P6 and P56 adipocytes to the synthetic dsDNA poly dA:dT (pdA:dT) packed in LyoVec (5 μg/ml, 2 h). (**C**) *Left:* Scheme of LyoVec encapsulated VACV-70 (Vaccinia virus DNA sequence), a ligand for IFI16 in human and p204/p205 in mouse. Responsiveness of P6 and P56 adipocytes to 1 μg/ml VACV-70 (18 h). (**D**) *Left:* Structure of cGAMP and scheme of its entry into the cytosol mediated by the solute carrier SLC19a (20). Transcript level of *Slc19a1* was equivalent in P6 and P56 iAT. *Right:* IFN-response of P6 and P56 iAT after cGAMP treatment (10 μg/ml, 18 h). **P*<0.05, ***P*<0.01, ****P*<0.001. Student's 2-tailed unpaired *t*-test or one-way ANOVA with Dunnett's post-hoc test.

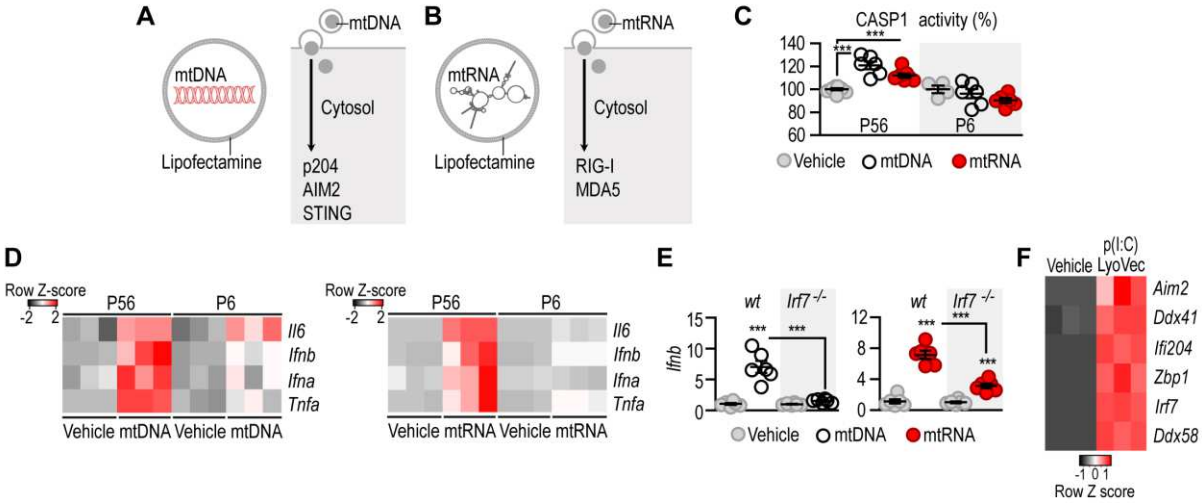

Supplemental Figure 4. Cytosolic mtDNA/mtRNA sensing in adipocytes

(**A**) Scheme of lipofectamine-encapsulated total mtDNA and its delivery into the cytosol of adipocytes. Cytosolic mtDNA is recognized by p204 (IFI16 in humans) and AIM2, and ultimately activates inflammasome and STING signaling. (**B**) Scheme of lipofectamine-encapsulated total mtRNA and its delivery into the cytosol of adipocytes. Cytosolic mtRNA activates RIG-I and MDA5 signaling. (**C**) Inflammasome activation of P56 and P6 adipocytes after 4-h challenge with cytoplasmic mtDNA or mtRNA. CASP1: caspase-1 of the inflammasome (**D**) IFN-response of P56 and P6 adipocytes following transfection with mtDNA or mtRNA (2 µg/ml, 18 h). (**E**) *Ifnb* transcription of wild-type (*wt*) and *Irf7*$^{-/-}$ adipocytes following transfection with vehicle, mtDNA or mtRNA (2 µg/ml, 4 h). (**F**) Transcription of the STING/AIM2 pathway, *Ddx58* and *Irf7* following 18-h activation of IRF7 signaling with LyoVec-encapsulated p(I:C). **P*<0.05, ***P*<0.01, ****P*<0.001. Student's 2-tailed unpaired *t*-test or one-way ANOVA with Dunnett´s post-hoc test.

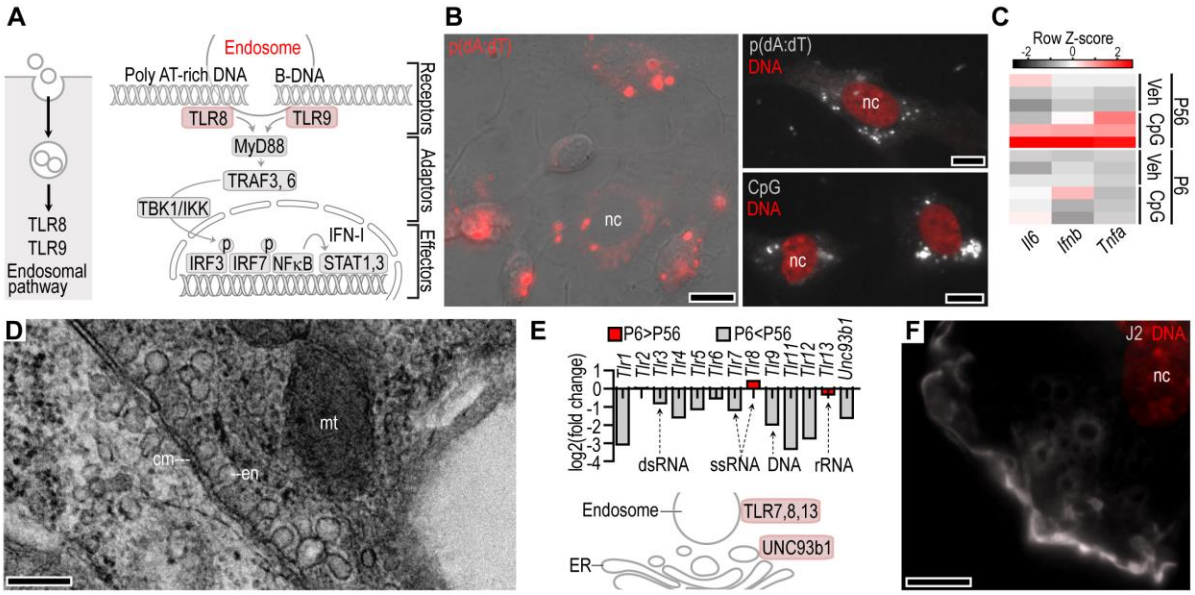

Supplemental Figure 5. Endosomal DNA/RNA sensing in adipocytes

(**A**) Scheme of DNA sensing pathways activated by endosomal uptake of DNA. (**B**) Rhodamine-conjugated naked DNA molecules (p(dA:dT) and CpG) were readily taken up by P6 adipocytes. Scale: 10 μm. (**C**) Effect of naked CpG on inflammatory gene expression in P6 and P56 adipocytes. (**D**) TEM image of two adjacent adipocytes *in vitro*. The cell membranes form numerous endosomes allowing the interchange of EV cargos. en: endosomes; mt: mitochondria; scale: 1 μm. (**E**) Transcript level of TLRs in P6 and P56 iAT. Respective ligands (dsRNA, ssRNA, DNA and rRNA) of the receptors are indicated. Mitochondrial RNA stimulates human TLR8 (21) and triggers inflammation in mouse macrophages mediated by TLR9 (22). (**F**) J2 antibody labeling of dsRNA at the lamellipodia of adipocytes, in an active region of endocytosis (23). nc: nucleus, scale: 10 μm.

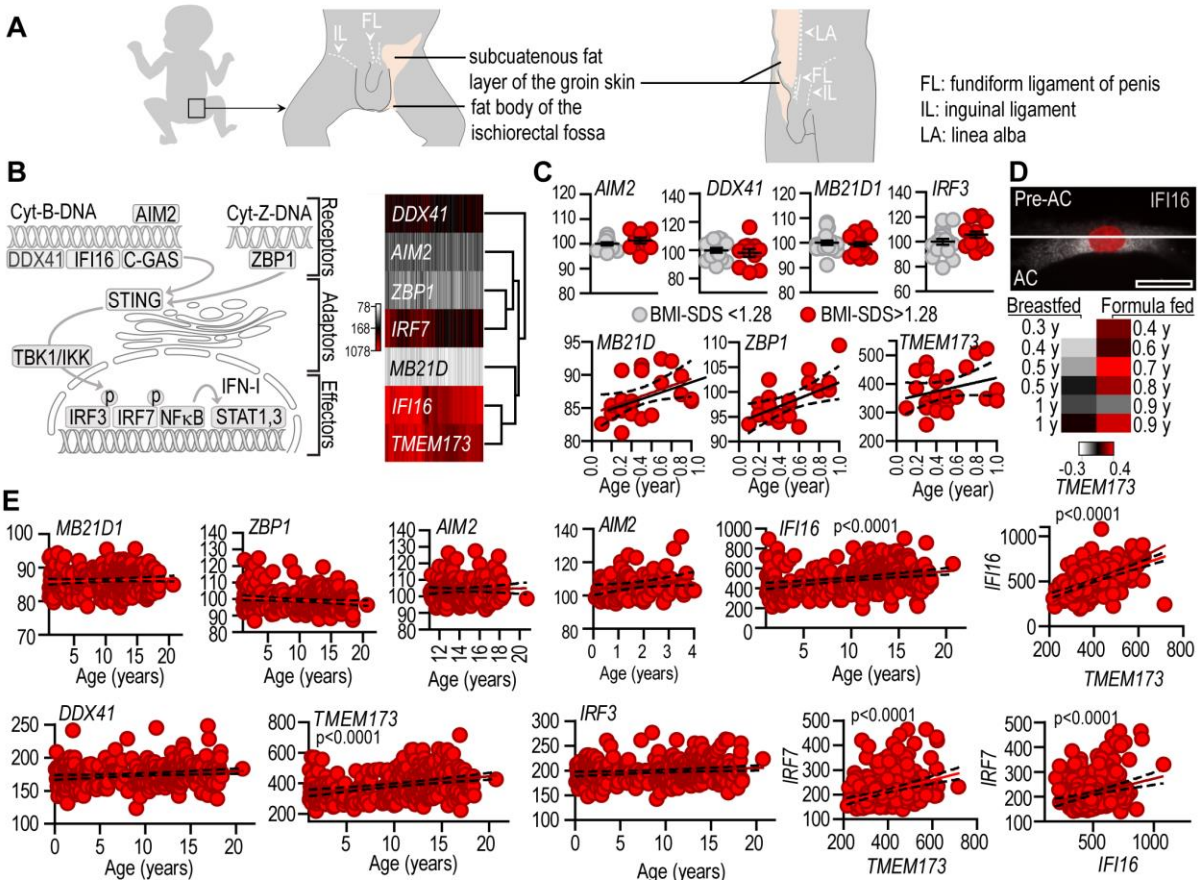

Supplemental Figure 6. STING/AIM2 pathways in human adipose tissue

(**A**) Anatomical sites of human inguinal adipose tissue (iAT) samples used in this study. *Left:* in infants, and *Right*: in children and adults. For proper comparison we used equivalent fat depots in all age groups, from the region bordered by the inguinal ligament, the fundiform ligament of the penis, and the linea alba. (**B**) Scheme of human STING/AIM2 pathways and the relative abundance of their gene products in the iAT collected from human infants (0.2–1.0 years of age, N=24), toddlers (1.1–2.0 years, N=29), children (3.0–11.0 years, N=99), adolescents and young adults (11.1–20.5 years, N=155). (**C**) *Top:* transcript level of adipose tissue *AIM2*, *DDX41*, *MB21D* (encoding cGAS) and *IRF3* in lean (BMI-SDS<1.28) and overweight or obese (BMI-SDS>1.28) infants and children; Illumina HT12v4 assay. *Bottom:* Correlation of age in years (y) and the transcript level of adipose tissue STING/AIM2 pathway genes in human infants. (**D**) *Top:* Immunostaining of IFI16 in a human preadipocyte (Pre-AC) and white adipocyte (AC). Samples from studies (14) and (24). Scale: 50 μm. *Bottom:* Level of adipose tissue *TMEM173* in breastfed and formula-fed infants. Formula-fed infants show premature loss of beige adipocytes in the subcutaneous fat depot (14). (**E**) Transcript level of the human adipose tissue STING/AIM2 pathway genes at various age groups. Correlation between *TMEM173* expression and the level of various DNA sensors. Age group: 0.1–20.5 years. Gender, gestational age, maternal age, maternal diabetes were not correlated with the above parameters. Linear regression analyses with Pearson's correlation.

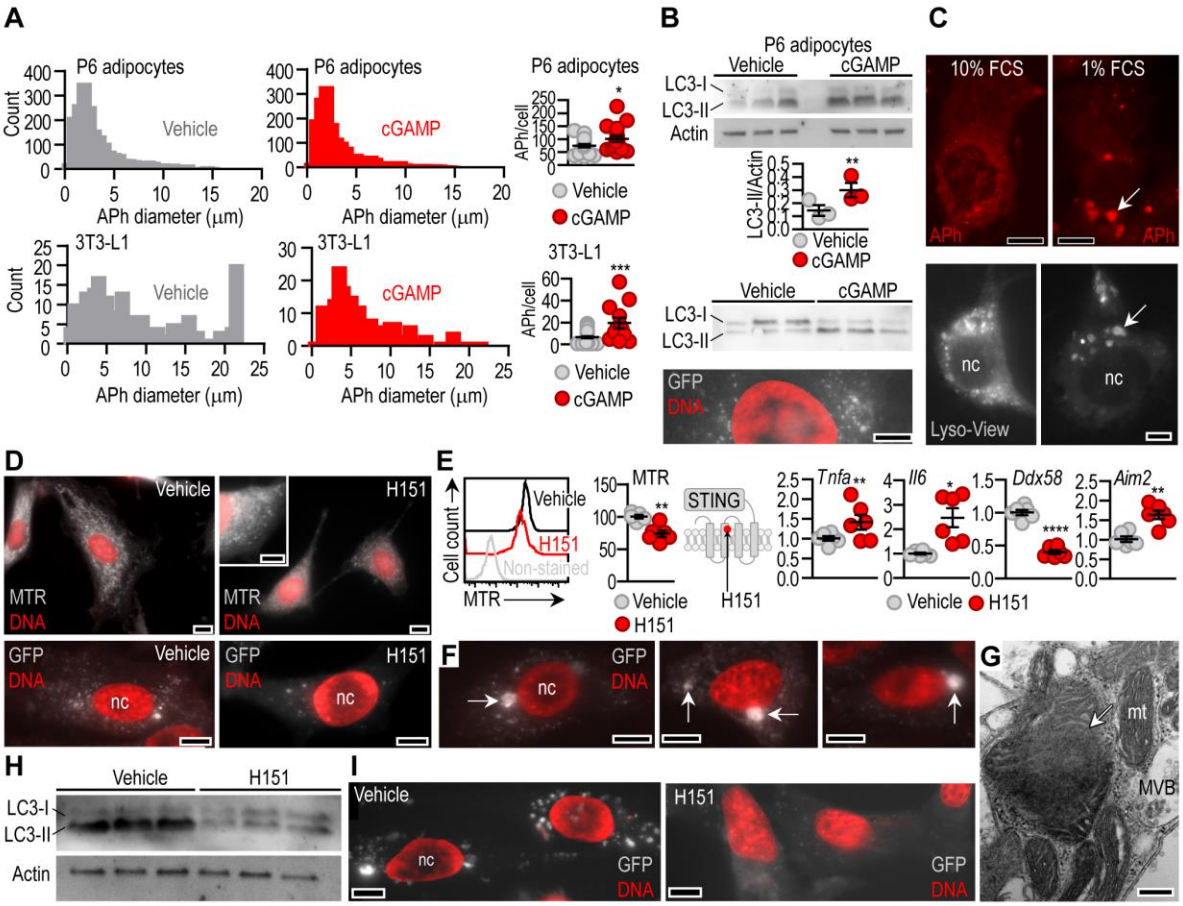

Supplemental Figure 7. STING-mediated mitophagy in P6 adipocytes

(**A**) Autophagosome (APh) number and size in P6 adipocytes and in 3T3-L1 adipocytes treated with vehicle or 5 μg/ml cGAMP for 6h. (**B**) *Top:* Western blotting of LC3 in P6 adipocytes and 3T3-L1 cells treated with vehicle or cGAMP (5 μg/ml, 6 h). *Bottom:* GFP-labeled mitochondrial remnants accumulate in autophagosomes after cGAMP treatment. Scale: 10 μm. (**C**) Autophagosomes and lysosomes (labeled with Lyso-View) in 3T3-L1 cells cultured in 10% fetal calf serum (FCS) or in 1% FCS-containing medium for 18 h. (**D**) Effect of STING inhibition with 0.5 μM H151 on mitochondrial content and morphology in P6 adipocytes. MTR: MitoTracker Red labeling, GFP: GFP labeling of newly synthesized mitochondria with the BacMam 0.2 labeling system, nc: nucleus; scale: 10 μm. (**E**) FACS analysis of MTR labeling of P6 adipocytes, and transcription of inflammatory genes and DNA sensors after 18-h H151 treatment. H151 covalently binds to STING (25). *Ddx58* encodes RIG-I. (**F**) Autophagosomes (arrows) containing GFP-labeled mitochondrial remnants in P6 adipocytes. Scale: 10 μm. (**G**) TEM image of an autophagosome containing mitochondria. mt: mitochondria, MVB: multivesicular body, arrow indicates autophagosome with mitochondrial remnants. Scale: 500 nm. (**H**) Western blotting of LC3 in P6 adipocytes following 6-h serum deprivation. Cells were treated with vehicle or H151 during serum deprivation. (**I**) GFP-labeled mitochondrial remnants in autophagosomes of P6 adipocytes following 6-h serum deprivation. Cells were treated with vehicle or H151 during serum deprivation. Scale: 10 μm. **P*<0.05, ***P*<0.01, ****P*<0.001. Student's 2-tailed unpaired *t*-test.

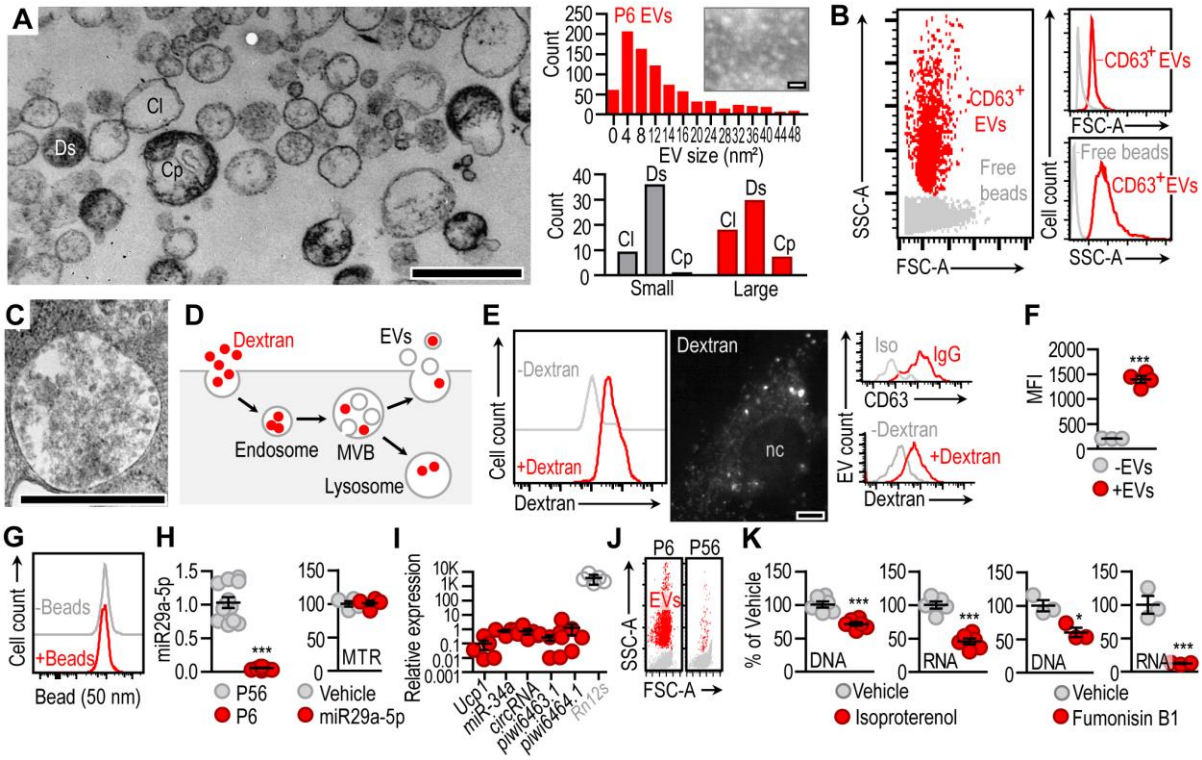

Supplemental Figure 8. Biogenesis of EVs by P6 adipocytes

(**A**) TEM image of EVs released by P6 adipocytes *in vitro*. Scale: 1 μm. Three distinct EV morphologies were recognized: electron-lucent or clear (Cl), electron-dense (Ds) and complex (Cp) EVs. Electron-lucent appearance is typical for EVs (26). Electron-dense EVs may be frequent in EVs within multivesicular bodies (MVBs) (27). Complex EVs contain remnants of intracellular membranes. Size distribution of P6 EVs; *inset* showing negative TEM staining of EVs. Scale: 100 nm. EVs were classified in small and large categories according to a recent study (28). (**B**) FACS analysis of EVs secreted by P6 adipocytes. Free beads: remainder of capture beads used to enrich EVs. (**C**) TEM image of an MVB; scale: 1 μm. (**D**) Endosomal pathway of EV generation was tested by incubating P6 adipocytes with FITC-conjugated dextran, a marker of fluid-phase endocytosis (pinocytosis). Dextran is taken up by endosomes and may later accumulate in MVBs or in lysosomes. (**E**) *Left:* FACS analysis of P6 adipocytes cultured without FITC-conjugated dextran (-Dextran) or after incubation with dextran (+Dextran). *Right:* P6 adipocytes readily endocytosed FITC-dextran, as confirmed with fluorescence microscopy. nc: nucleus; scale: 10 μm. EVs secreted by the dextran-incubated adipocytes were collected and analyzed further with FACS. Dextran was present in the EVs, showing that the endosomal pathway contributed to EV generation. (**F**) Adipocytes were incubated without EVs (-EVs) or with FITC dextran-labeled EVs (+EVs) for 4h. Mean fluorescence intensity (MFI) of the adipocytes was measured by FACS, confirming the uptake of EV cargo by adipocytes. (**G**) Phagocytosis activity of P6 adipocytes was tested with using 50-nm large latex beads. Adipocytes failed to phagocytose these particles, showing that EVs were not taken up by phagocytosis. (**H**) Level of an adipose tissue mesenchymal stem cell-specific microRNA (miR-29a-5p) in P6 and P56 EVs (29). Effect of miR-29a-5p overexpression of the mitochondrial content (MTR fluorescence intensity). (**I**) *Ucp1* and small non-coding RNA species in the EV cargo of P6 adipocytes. As a comparison, the level of the mitochondrially-encoded 12S ribosomal RNA *(Rn12s)* is shown. (**J**) FACS plots of EVs secreted by P6 and P56 adipocytes. (**K**) Inhibitors of EV generation reduced the DNA and RNA content in the culture medium of P6 adipocytes. Isoproterenol (1 μM) inhibits EV release (30), and fumonisin B1 (30 μM) inhibits ceramide synthase, a key enzyme of negative budding of MVBs (31).

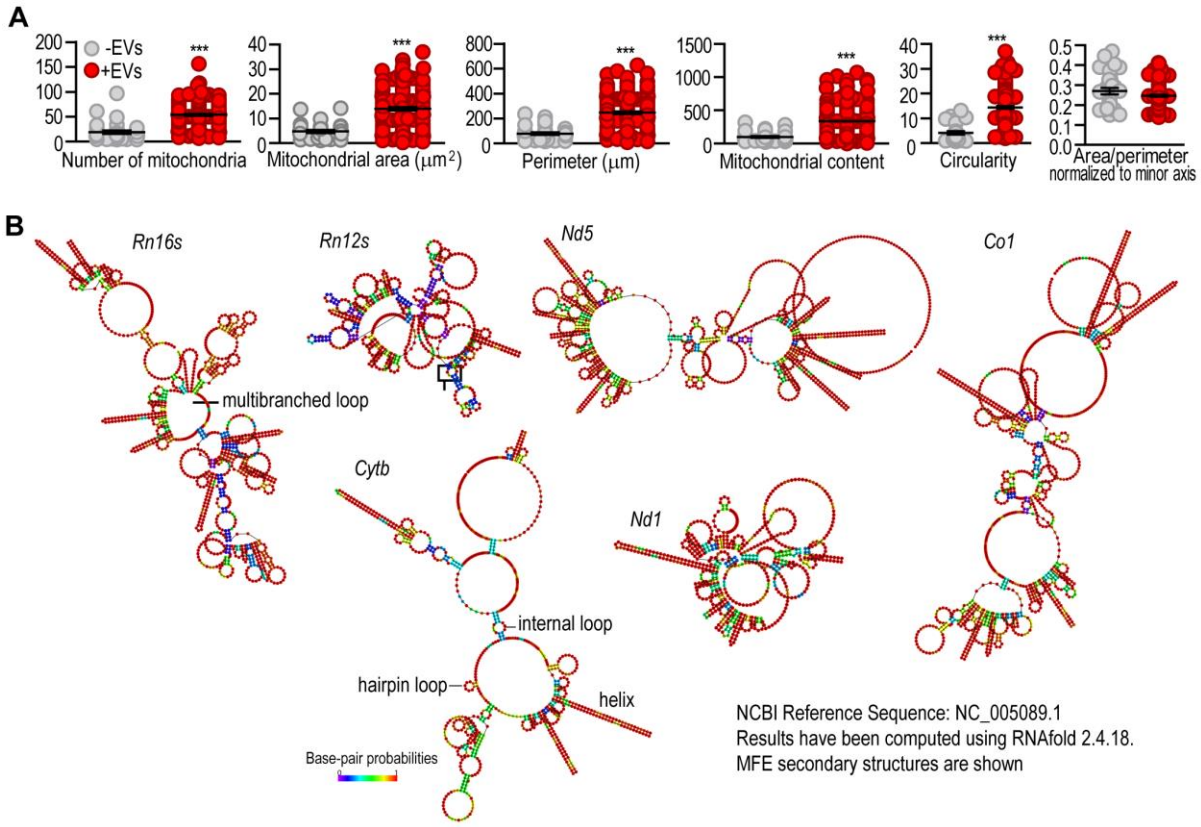

Supplemental Figure 9. Effect of adipocyte EV cargo on mitochondrial morphology, and predicted secondary structure of mtRNA species found in adipocyte EVs
(**A**) Mitochondrial morphometry of 3T3-L1 cells without extracellular vesicles (-EVs) or with P6 EVs (+EVs). ***$P<0.001$. Student's 2-tailed unpaired *t*-test. (**B**) Predicted minimum free energy (MFE) secondary structures of mtRNA species found in P6 EVs. Results were computed using ViennaRNA Package 2.0 and RNAfold 2.2.18, as described (32, 33).

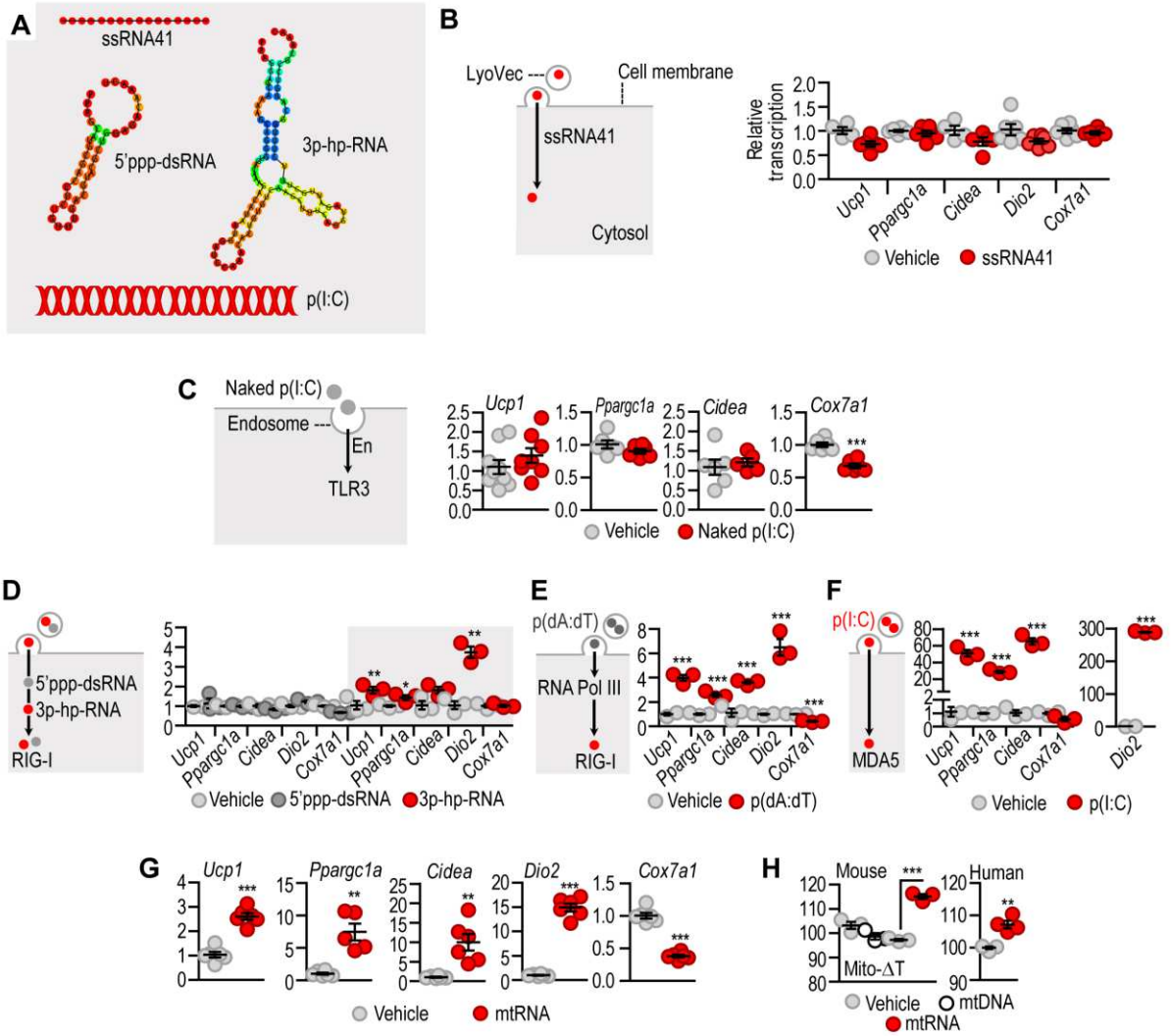

Supplemental Figure 10. Cytosolic and endosomal RNA effects on mitobiogenesis

(A) Secondary and schematic structures of the synthetic ligands used to activate cytosolic RNA sensors. ssRNA41: single-stranded RNA, 3p-hp-RNA: 5' triphosphate hairpin RNA, is an RIG-I ligand (34), 5'ppp-dsRNA: 5' triphosphate dsRNA, a ligand for RIG-I, cytosolic p(I:C) activates MDA5 and RIG-I (35), and cytosolic p(dA:dT) is transcribed into RNA and ultimately activates RIG-I (36). (**B**) Adipocytes were transfected with 2 μg/ml ssRNA41 using the LyoVec transfection system for cytosol delivery. Levels of beige marker genes was measured 18 h after transfection. (**C**) 3T3-L1 cells were treated with 5 μg/ml naked pI:pC to stimulate TLR3 and beige adipocyte gene transcription was then measured 18h after treatment. (**D**,**E**,**F**) Adipocytes were transfected with RIG-I/MDA5 ligands: 5'ppp-dsRNA, 3p-hairpin-RNA, p(dA:dT) and p(I:C) in LyoVec. Levels of beige marker genes was measured 18 h after transfection. (**G**) Transcript level of beige adipocyte genes in P56 adipocytes transfected with mtRNA for 18h. (**H**) Mitochondrial temperature change (Mito-ΔT) measured with the heat-sensitive probe Mitothermo-Yellow (MTY) in mouse and human primary adipocytes. Adipocytes were transfected with vehicle, mtDNA or mtRNA for 18 h. **P*<0.05, ***P*<0.01, ****P*<0.001. Student's 2-tailed unpaired *t*-test.

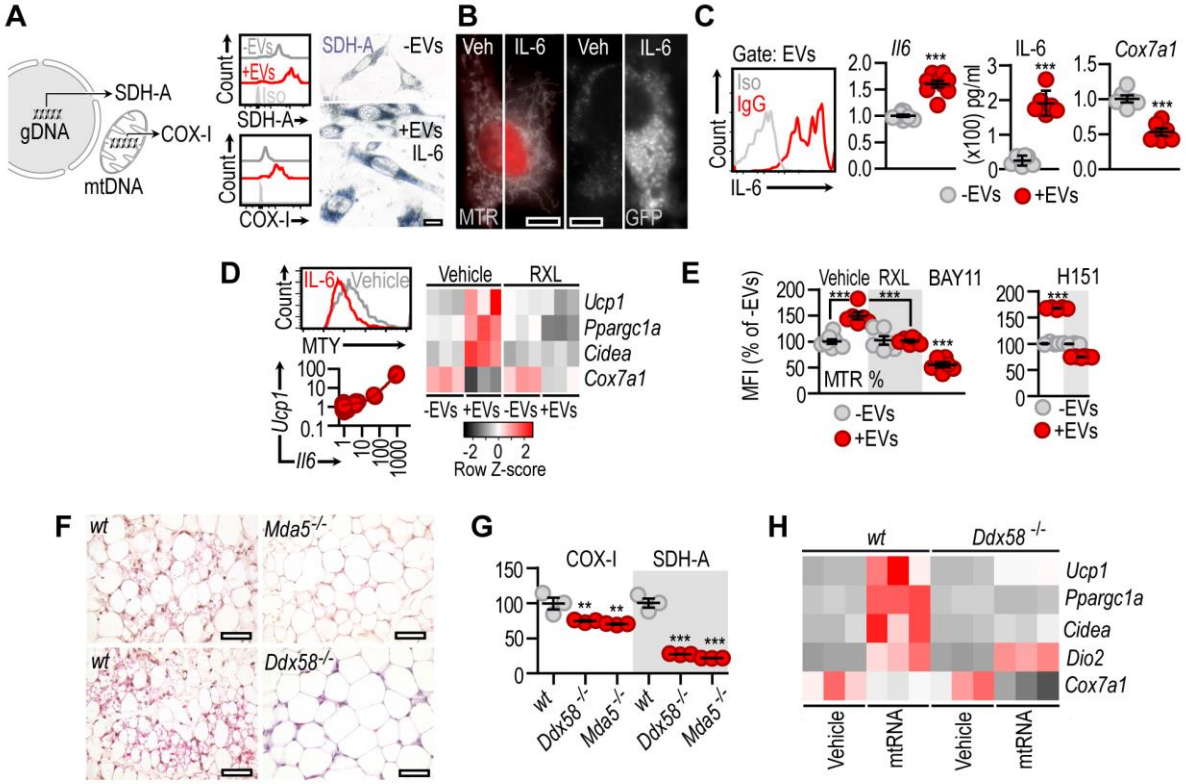

Supplemental Figure 11. IL-6/STAT3 and RIG-I/MDA5 signaling and mitobiogenesis
(**A**) Mitobiogenesis was assessed by measuring SDH-A (succinate dehydrogenase complex, subunit A) and COX-1 (cyclooxygenase 1) by FACS. SDH-A is encoded by genomic DNA (gDNA), COX-I by mtDNA. Representative FACS histograms of COX-I and SDH-A in 3T3-L1 cells after P6 EV treatment. Histochemical staining of SDH-A activity of 3T3-L1 cells cultured without EVs (-EVs), with P6 EVs (+EVs) or with 0.2 ng/ml IL-6 for 18 h. Scale: 10 µm. (**B**) Effect of 200 pg/ml IL-6 on the net mitochondrial mass labeled with MitoTracker Red (MTR), and on the amount of newly synthesized (GFP-expressing) mitochondria. Scale: 50 µm. (**C**) FACS analysis of IL-6 content of P6 EVs. Iso: isotype control; IgG: labeling with anti-IL-6 IgG. Effect of P6 EVs on adipocyte *Il6* expression and IL-6 release. Effect of P6 EVs on *Cox7a1* expression (**D**) Effect of 200 pg/ml IL-6 on the Mitothermo-Yellow (MTY) signal in 3T3-L1 cells. Correlation of *Il6* and *Ucp1* relative expression in adipocytes. Heat map showing expression levels of beige adipocyte genes in 3T3-L1 cells treated with P6 EVs for 18 h. (**E**) MTR signal in 3T3-L1 cells treated with P6 EVs for 18 h. RXL: cells were simultaneously treated with the JAK2/STAT3 inhibitor ruxolitinib; BAY11-7082: cells were treated with an NFκB inhibitor to abrogate the effect of IL-6. (**F**) Histology of iAT from wild-type (*wt*), RIG-I-deficient (*Ddx58*$^{-/-}$) and MDA5-deficient (*Mda5*$^{-/-}$) mice. Note the absence of beige (multilocular) adipocytes in *Ddx58*$^{-/-}$ and *Mda5*$^{-/-}$ mice. Scale 50 µm. (**G**) Mitobiogenesis (relative COX-I and SDH-A levels) in *wt*, *Ddx58*$^{-/-}$ and *Mda5*$^{-/-}$ adipocytes. (**H**) Heat map showing expression levels of beige adipocyte genes in *wt* or *Ddx58*$^{-/-}$ adipocytes treated with vehicle or mtRNA for 18 h. **P*<0.05, ***P*<0.01, ****P*<0.001. Student's 2-tailed unpaired *t*-test.

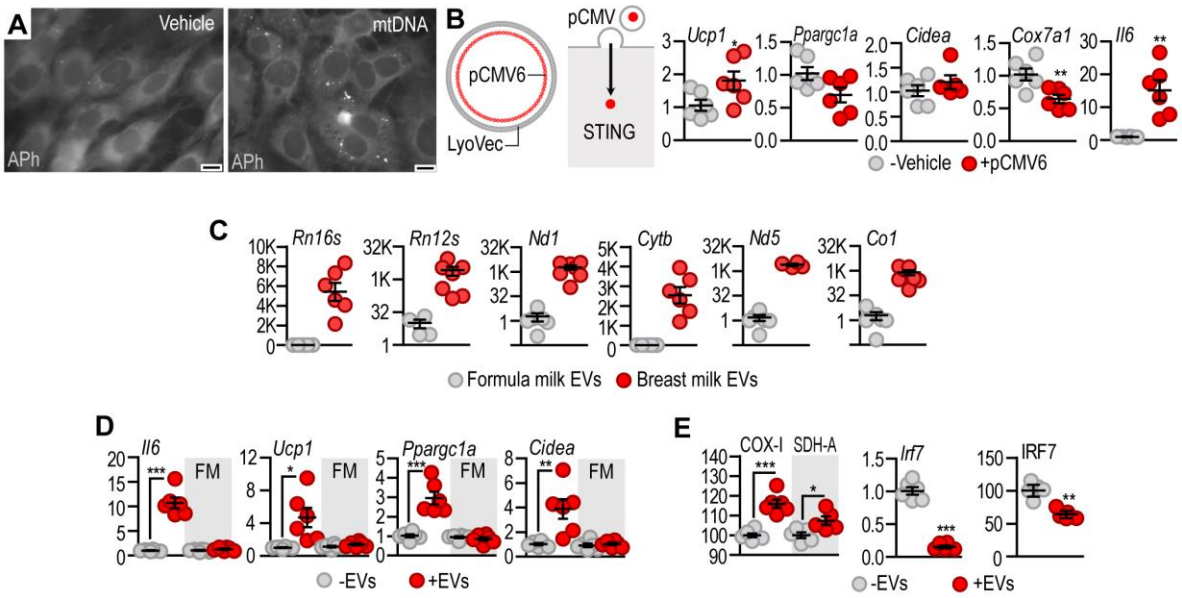

Supplemental Figure 12. Cytosolic DNA/RNA effects on mitobiogenesis

(**A**) Autophagosomes (APh) in P6 adipocytes treated with vehicle or transfected with 2 μg/ml total mtDNA for 18 h. Scale: 10 μm. (**B**) Scheme of LyoVec-encapsulated pCMV6 plasmid – an activator of the c-GAS/STING pathway – and its effect on beige adipocyte gene expression in P6 adipocytes. (**C**) Relative abundance of mtRNA species in human breast milk EVs and commercially available formula milk EVs. (**D**) Effect of breast milk EVs on beige adipocyte gene expression in P56 adipocytes. As a comparison, adipocytes were treated with formula milk-derived EVs (FM). (**E**) Effect of breast milk EVs on the mitobiogenesis of human subcutaneous adipocytes, *Irf7* mRNA levels in mouse adipocytes, and IRF7 protein levels of human adipocytes. Adipocytes were treated with breast milk-derived EVs for 18 h. COX-I: cytochrome oxidase, SDH-A: succinate dehydrogenase, **P*<0.05, ***P*<0.01, ****P*<0.001. Student's 2-tailed unpaired *t*-test.

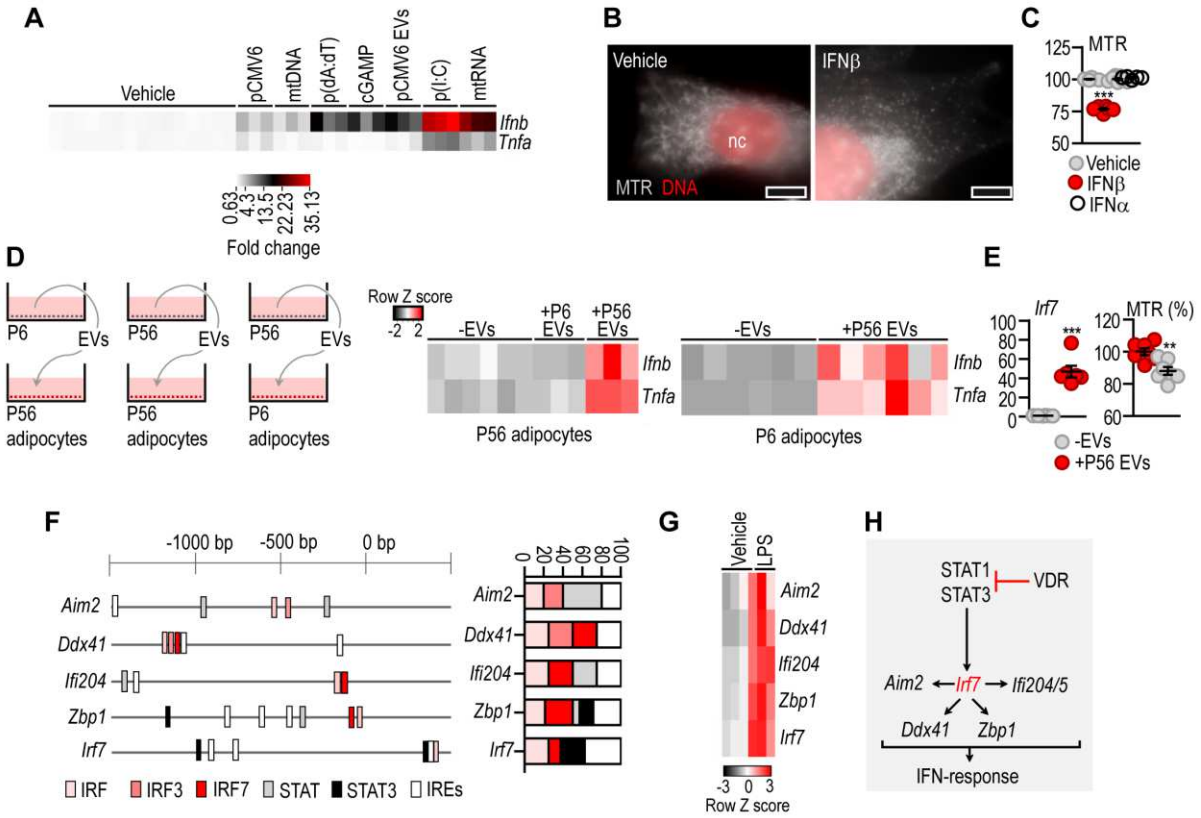

Supplemental Figure 13. IFN-response to EV cargo in adipocytes

(**A**) Effect of cytosolic DNA/RNA on *Ifnb* expression in P56 adipocytes. pCMV6: transfection with pCMV6 plasmid (circular cytosolic DNA), pCMV6 EVs: treatment with extracellular vesicles released by pCMV6 plasmid-transfected adipocytes) (**B**) Effect of IFNβ on the mitochondrial network in P56 adipocytes. Scale: 20 μm. (**C**) Effect of IFNβ and IFNα on mitochondrial mass measured by MitoTracker Red (MTR) staining intensity. Cells were treated with vehicle, 1 pg/ml IFNβ or 1 pg/ml IFNα for 18 h. (**D**) EVs of P6 adipocytes were collected and added to cultures of P56 adipocytes. Similarly, EVs of P56 adipocytes were collected and added to P56 or P6 adipocytes. Levels of *Ifnb* and *Tnfa* were then measured. P6 EVs did not induce IFN-response, whereas P56 EVs triggered a robust IFN-response. (**E**) Transcript level of *Irf7*, and MTR staining intensity in P6 adipocytes treated with P56 EVs. Unlike P6 EVs, which suppressed *Irf7*, P56 EVs stimulated robust *Irf7* expression (see Figure 3C) and reduced mitochondrial content. (**F**) Relative position and percentage of transcription factor binding sites in the promoters of the AIM2/STING pathway and *Irf7*. (**G**) Effect of LPS on the transcription of AIM2/STING pathway and *Irf7* in adipocytes. (**H**) Scheme of the VDR-suppressed signal path which control the expression of *Irf7*, AIM2/STING pathway and IFN-response to cytosolic DNA/RNA (37-40).

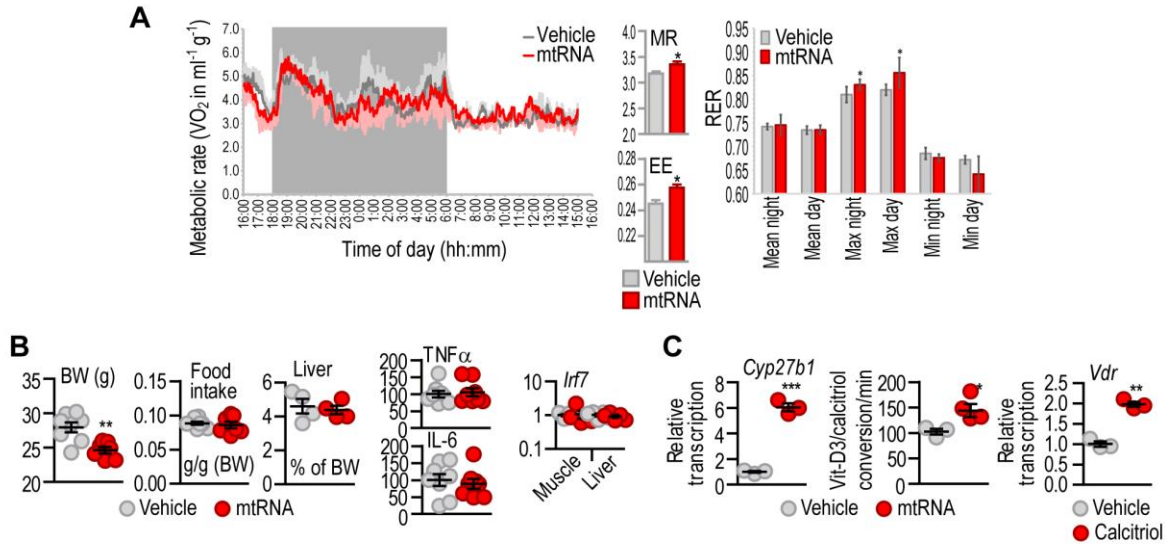

Supplemental Figure 14. Metabolic role of mtRNA-mediated signaling
(**A**) Indirect calorimetry assay of HFD-fed adult male C57BL/6 mice. The inguinal fat depot was transfected with vehicle or with 0.6 μg/g body weight (BW) per day mtRNA for 14 days. The mtRNA was delivered into the adipocyte cytoplasm using magnetofection. Both groups received 4 ng/g BW Vit-D3 daily. MR: metabolic rate, EE: energy expenditure, RER: respiratory exchange rate (**B**) BW, daily food intake normalized to BW, and liver weight normalized to BW. Plasma level of TNFα and IL-6 (% of vehicle) from vehicle- or mtRNA-transfected mice, and the level of *Irf7* in quadriceps muscle and liver. (**C**) *Left:* Transcription of *Cyp27b1* (encoding a Vit-D3/calcitriol converting mitochondrial enzyme) in adipocytes treated with vehicle or transfected with mtRNA for 18h. *Middle:* Rate of Vit-D3/calcitriol conversion in the same cells. *Right:* Effect of calcitriol on the transcription of *Vdr* in adipocytes. **P*<0.05, ***P*<0.01, ***P<0.001. Student's 2-tailed unpaired *t*-test.

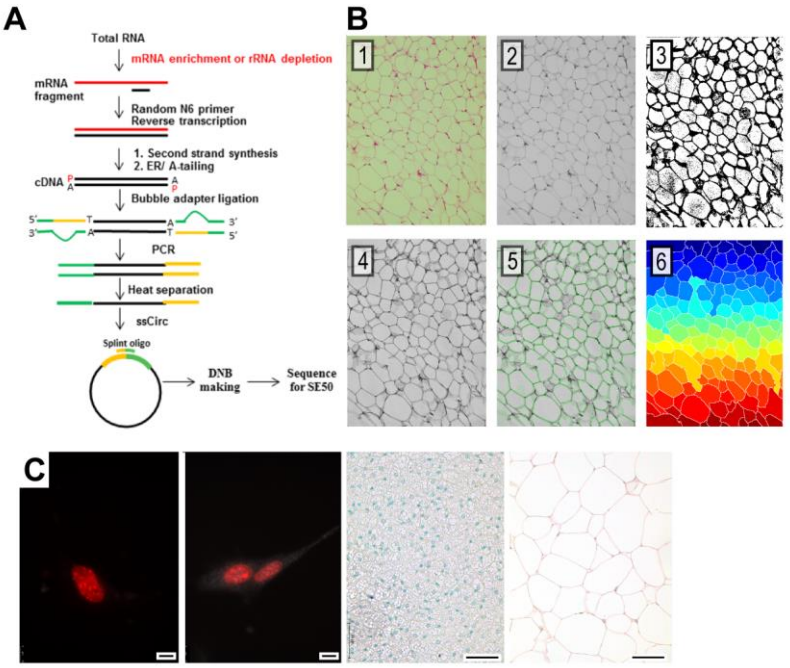

Supplemental Figure 15. Technical information on next-generation sequencing and image analysis

(**A**) Work flow of the next-generation sequencing analysis. (**B**) Steps of image analysis in histomorphometry. (**C**) Negative control specimens. *Left:* Adipocytes *in vitro*, stained with secondary antibodies only; nuclei are labeled with DAPI. Scale: 10 µm. *Middle:* Brown adipose tissue section labeled with secondary antibody only. Scale: 20 µm. Right: human adipose tissue labeled with secondary antibody only. Scale: 20 µm.

Supplemental Table 1. Mouse qPCR primer sequences used in the study

Bactin	fw	GCACCAGGGTGTGATGGTG
	rev	CCAGATCTTCTCCATGTCGTCC
Ppia	fw	ATTTCTTTTGACTTGCGGGC
	rev	AGACTTGAAGGGGAATG
Gapdh	fw	TGACGTGCCGCCTGGAGAAA
	rev	AGTGTAGCCCAAGATGCCCTTCAG
Aim2	fw	GATTCAAAGTGCAGGTGCGG
	rev	TCTGAGGGTTAGCTTGAGGAC
Ddx41	fw	ACAGGAGAAGCGGTTGCCTTTC
	rev	GACGGCAGTAATACTCCAGGATG
Ifi204	fw	CAGGGAAAATGGAAGTGGTG
	rev	CAGAGAGGTTCTCCCGACTG
Zbp1	fw	AACCCTCAATCAAGTCCTTTACCGC
	rev	TCTTCCACGTCTGTCCGTCATAGCT
Mb21d	fw	AGGAAGCCCTGCTGTAACACTTCT
	rev	AGCCAGCCTTGAATAGGTAGGTAGTCCT
Tmem173	fw	GGGCCCTGTCACTTTTGGTC
	rev	GAGTATGGCATCAGCAGCCAC
Irf3	fw	GGCTTGTGATGGTCAAGGTT
	rev	CATGTCCTCCACCAAGTCCT
Irf7	fw	CGACTTCAGCACTTTCTTCCGAGA
	rev	AGATGGTGTAGTGTGGTGACCCTT
Il6	fw	GCTACCAAACTGGATATAATCAGGA
	rev	CCAGGTAGCTATGGTACTCCAGAA
Tnfa	fw	TGCCTATGTCTCAGCCTCTTC
	rev	GAGGCCATTTGGGAACTTCT
Ifnb	fw	CCAGCTCCAAGAAAGGACGA
	rev	CGCCCTGTAGGTGAGGTTGAT
Ifna	fw	TGAAGGACAGGAAGGACTTTG
	rev	GAATGAGTCTAGGAGGGTTGT
28S	fw	CAGGGGAATCCGACTGTTTA
	rev	ATGACGAGGCATTTGGCTAC
18S	fw	CGCGGTTCTATTTTGTTGGT
	rev	AGTCGGCATCGTTTATGGTC
16S	fw	ACACCGGAATGCCTAAAGGA
	rev	ATACCGCGGCCGTTAAACTT
12S	fw	ACACCTTGCCTAGCCACACC
	rev	GTGGCTGGCACGAAATTTACCA
Nd1	fw	GCTTTACGAGCCGTAGCCCA
	rev	GGGTCAGGCTGGCAGAAGTAA
Cytb	fw	TCCTTCATGTCGGACGAGGC
	rev	AATGCTGTGGCTATGACTGCG
Nd5	fw	GGCCCTACACCAGTTTCAGC
	rev	AGGGCTCCGAGGCAAAGTAT
Co1	fw	TCAACATGAAACCCCCAGCCA
	rev	GCGGCTAGCACTGGTAGTGA

Ucp1	fw	CCTGCCTCTCTCGGAAACAA
	rev	CTGTAGGCTGCCCAATGAAC
Ppargc1	fw	GACTCAGTGTCACCACCGAAA
	rev	TGAACGAGAGCGCATCCTT
Cox7a1	fw	ATGAGGGCCCTACGGGTCTC
	rev	CATTGTCGGCCTGGAAGAG
Cidea	fw	TACTACCCGGTGTCCATTTCT
	rev	ATCACAACTGGCCTGGTTACG
Dio2	fw	GTCCGCAAATGACCCCTTT
	rev	CCCACCCACTCTCTGACTTTC
Ifi205	fw	CAAGCAGGCCACTTCTGTTG
	rev	TCAAACGGGTCTGTTGCAGT
Ddx58	fw	CAAACCGGGCAACAGGAATG
	rev	ATCTCCGCTGGCTCTGAATG
Ifi202b	fw	AAGTTCCCGGCTTGCAGAAC
	rev	TCCAGGAGAGGCTTGAGGTT
Mndal	fw	GACAGCACACTAGAAACCCC
	rev	CTTGTCCTCCATCCAGTCCG
miR34a	fw	TCTTTGGCAGTGTCTTAGCTGG
	rev	ACAATGTGCAGCACTTCTAGGG
circRNA	fw	CTGCTCCTCCAGCTCTT
	rev	AGTGATCTTGAACCCCAAAG
piRNA 6464.1	fw	GGCAAGCTTAGGAGGTGTCC
	rev	CGTGGGTCCACTGTATCACC
piRNA 6463.1	fw	TAAAGCCCTAAAGCCCACGG
	rev	AGGTGTAATGCCAGCCAGTC
Pnpt1	fw	CTTGGACATGGTGCTCTTGC
	rev	GCCAAACTTCCACCACATGC
Adrb3	fw	GTCGTCTTCTGTGTAGCTACGGT
	rev	CATAGCCATCAAACCTGTTGAG
Lipe (Hsl)	fw	AGCCTCATGGACCCTCTTCT
	rev	AGCGAAGTGTCTCTCTGCAC
Atg (Pnpla2)	fw	ACTGAACCAACCCAACCCTT
	rev	CGCACTGGTAGCATGTTGGA
Cyp27b1	fw	AGCTCCTGCGACAAGAAAGT
	rev	ATTCTTCACCATCCGCCGTTA
Vdr	fw	ACTTTGACCGGAATGTGCCT
	rev	CATGCTCCGCCTGAAGAAAC

Supplemental Table 1. (cont.) qPCR primers for measuring mouse mtDNA

Nd1	fw	GCTTTACGAGCCGTAGCCCA
	rev	GGGTCAGGCTGGCAGAAGTAA
16S	fw	ACACCGGAATGCCTAAAGGA
	rev	ATACCGCGGCCGTTAAACTT
12S	fw	ACACCTTGCCTAGCCACACC
	rev	GTGGCTGGCACGAAATTTACCA
D-loop	fw	AATCTACCATCCTCCGTGAAACC
	rev	TCAGTTTAGCTACCCCCAAGTTTAA
Cytb	fw	TCCTTCATGTCGGACGAGGC
	rev	AATGCTGTGGCTATGACTGCG
Atp6	fw	AGCTCACTTGCCCACTTCCT
	rev	AAGCCGGACTGCTAATGCCA
Nd5	fw	GGCCCTACACCAGTTTCAGC
	rev	AGGGCTCCGAGGCAAAGTAT
Co1	fw	TCAACATGAAACCCCCAGCCA
	rev	GCGGCTAGCACTGGTAGTGA
HK2	fw	GCCAGCCTCTCCTGATTTTAGTGT
	rev	GGGAACACAAAAGACCTCTTCTGG

Supplemental Table 1. (cont.) qPCR primers for measuring bovine/human mtRNA

16S	fw	GACTTCACCAGTCAAAGCGA
	rev	ACATCGAGGTCGTAAACCCT
12S	fw	ACTGCTCGCCAGAACACTAC
	rev	GGTGAGGTTGATCGGGGTTT
ND1	fw	GCAGCCGCTATTAAAGGTTCG
	rev	TATCATTTACGGGGGAAGGCG
ND5	fw	TATGTGCTCCGGGTCCATCA
	rev	CTGCTAATGCTAGGCTGCCA
CO1	fw	TCAGGCTACACCCTAGACCA
	rev	CCGGATAGGCCGAGAAAGTG
CYTB	fw	AACTTCGGCTCACTCCTTGG
	rev	CTCGAGTGATGTGGGCGATT

Supplemental Table 1. (cont.) qPCR primers for measuring bovine/human mtDNA

16S	fw	GACTTCACCAGTCAAAGCGA
	rev	ACATCGAGGTCGTAAACCCT
12S	fw	ACTGCTCGCCAGAACACTAC
	rev	GGTGAGGTTGATCGGGGTTT
ND1	fw	GCAGCCGCTATTAAAGGTTCG
	rev	TATCATTTACGGGGGAAGGCG
ND5	fw	TATGTGCTCCGGGTCCATCA
	rev	CTGCTAATGCTAGGCTGCCA
CO1	fw	TCAGGCTACACCCTAGACCA
	rev	CCGGATAGGCCGAGAAAGTG
CYTB	fw	AACTTCGGCTCACTCCTTGG
	rev	CTCGAGTGATGTGGGCGATT

Supplemental Table 2. Antibodies used in the study (h, human; m, mouse)

Target	Cat. No.	IgG type, source
h/m STING	NBP2-24683	Rabbit polyclonal Novus Biologicals, Denver, CO
h/m AIM2	201708-T10	Rabbit polyclonal Sino Biological, Eschborn, Germany
h/m DDX41	102459-T32	Rabbit polyclonal Sino Biological, Eschborn, Germany
h/m p204 (IFI16)	NBP2-27153	Rabbit Polyclonal Novus Biologicals, Denver, CO
h/m ZBP1	207744-T08	Rabbit polyclonal Sino Biological, Eschborn, Germany
h/m LC3	L8918	Rabbit polyclonal, Merck Sigma-Aldrich, St. Louis, MO, Darmstadt, Germany
h/m UCP1	PA1-24894	Rabbit polyclonal ThermoFisher Scientific, Rockford, IL
m NPFF	ab10352	Rabbit polyclonal Abcam, Cambridge, UK
β-actin	NB600-532SS	Rabbit polyclonal Novus Biologicals, Denver, CO
h/m DDX41	102459-T32	Rabbit polyclonal Invitrogen, Carlsbad, CA
h/m Tmem150b	PA5-71527	Rabbit polyclonal Invitrogen, Carlsbad, CA
J2 (dsRNA)	Anti-dsRNA [J2]	Mouse monoclonal Absolute Antibody, Wilton, UK
m IRF7	12-5829-82	PE-conjugated monoclonal IgG, and matching isotype IgG, ThermoFisher, Waltham, MA
m F4/80 antigen m CD11b	sc-377009 E-AB-F1081E	F4/80 APC, CD45 PerCy5.5, CD11b APC or PE or AF700 (FACS analysis), eBioscience, ThermoFisher, Waltham, MA, Santa Cruz Biotech (for IHC)
Rabbit anti-goat IgG	F-2765	H+L, cross-Adsorbed, FITC, polyclonal, secondary antibody, Invitrogen, Carlsbad, CA
Goat anti-rabbit IgG	A16096	Goat anti-Rabbit IgG (H+L), HRP-conjugated Invitrogen, Carlsbad, CA

Supplemental Methods

Activation and inhibition of cytosolic DNA/RNA sensors

To activate STING, we treated adipocytes or 3T3-L1 cells with cGAMP (InvivoGene, Toulouse, France) for 6–18 h, or overexpressed the pCMV6 plasmid (OriGene Technologies, Rockville, MD). In the latter case, 1 μg of DNA was transfected into 300,000 cells using TurboFect Transfection Reagent (Fisher Scientific, Hampton, NH). Control cells received transfection reagent only. Analyses were performed 18-h after transfection. To stimulate RIG-I/MDA5, we transfected 3T3-L1 cells at 80% confluency with high molecular weight polyinosine-polycytidylic acid (p(I:C)) or poly(deoxyadenylic-deoxythymidylic) acid (p(dA:dT)) using the LyoVec cationic lipid-based transfection reagent (InvivoGene, Toulouse, France). Control cells were treated with LyoVec transfection reagent only. We used 2.5–5 μg/ml p(dA:dT) or p(I:C), and cells were analyzed 2–24 h after transfection. IFI16/p204 was activated with 1 μg/ml VACV-70 conjugated to LyoVec transfection reagent (InvivoGene; 18 h) (41). Treatments are summarized in the table below.

Activation of cytosolic nucleic acid sensors with various ligands

Receptor	**Ligand**	**EC_{50}**	**Applied concentration**
STING	2´3 cGAMP	20 nM	10 μg/ml
cGAS	poly(dA:dT) 2h	40-200 ng/ml	2.5-5 μg/ml
	human/mouse mtDNA	-	2 μg/ml
	pCMV6 circular DNA	-	1 μg/well
RIG-I	3p-hpRNA	5 ng/ml	0.5 μg/ml
	5´ppp-dsRNA	1.2 nM	1 μg/ml
	poly(I:C) HMW	70±10 ng/ml	0.5 μg/ml
RIG-I and **MDA5**	poly(dA:dT) 18-24h	40-200 ng/ml	2.5-5 μg/ml
	low molecular weight poly(I:C)	82±8 ng/ml	1 μg/ml
	human/mouse mtRNA	-	2 μg/well
AIM2	poly(dA:dT) 2h	40-200 ng/ml	2.5-5 μg/ml
DDX41	poly(dA:dT) 2h	40-200 ng/ml	2.5-5 μg/ml
	dsDNA (VACV-70)	-	1 μg/ml
IFI16 (p204 or **Ifi204)**	poly(dA:dT) 2h	40-200 ng/ml	2.5-5 μg/ml
	dsDNA (VACV-70)	-	1 μg/ml
ZBP1	poly(dA:dT) 2h	40-200 ng/ml	2.5-5 μg/ml

TLR3 was stimulated with naked p(I:C) (Sigma-Aldrich, 10 ng/ml, 18 h) and TLR8/9 with naked p(dA:dT) or CpG (1 μg/ml synthetic oligonucleotides that contain unmethylated CpG dinucleotides; InvivoGene) for 8 h. STING was inhibited with the irreversible STING inhibitor H-151 (0.5 μM, InvivoGene) (25). As a negative control we used ssRNA (InvivoGene). NFκB was inhibited with 5 μM BAY 11-7082 and JAK2/STAT3 with 280 nM ruxolitinib (Cayman Chemical Company, Ann Arbor, MI). Mitochondrial damage was induced with 10 ng/ml LPS or with CCCP (carbonyl cyanide m-chlorophenyl hydrazone, 1 μM, 15 min treatment).

Vit-D3 and calcitriol were purchased from Sigma-Aldrich; IL-6, IFNα and IFNβ from ImmunoTools (Friesoythe, Germany), NPVF, human and mouse NPFF from Tocris Bioscience (Bristol, UK). Isoproterenol and fumonisin B1 were purchased from Sigma-

Aldrich and from Cayman Chemical Company, respectively. To test the inhibitory effect of Vit-D3 on IRF7 signaling, 3T3-L1 cells were treated with 1 μM Vit-D3 for 48 h, and treated further with vehicle or 5 μg/ml cGAMP for 6 h, or were transfected with mtRNA for 18 h. VDR was inhibited with PS121912, as described (42). Cellular uptake of cGAMP is dependent on the transporter Slc19a1 (20), whose level was similar in P6 and P56 adipocytes (GEO submission #GSE154925).

Isolation of extracellular vesicles from cell culture media, breast milk and formula milk

Extracellular vesicles (EVs) were collected from adipocyte culture media, human breast milk, or from commercially available cattle milk-based infant formula. Human breast milk was collected from healthy volunteers. For cell culture, to avoid contamination with bovine EVs, we used EV-depleted fetal calf serum throughout the study (Gibco). EVs were precipitated with the EPStep exosome precipitation solution (Immunostep, Centro de Investigación del Cáncer, Campus Miguel de Unamuno, Salamanca, Spain) and concentrated by centrifugation. EVs were analyzed with FACS using capture beads and labeling for CD63 (Immunostep). EV pellets were used for treating recipient cells, to extract DNA/RNA, or were processed for FACS. Fractions of EV pellets and adipocytes were also fixed in paraformaldehyde/glutaraldehyde, and processed for transmission electron microscopy (TEM) analysis, as described (43). Morphology of EVs was analyzed with conventional TEM, and with negative staining for TEM (44). EV diameter and area was measured with ImageJ (NIH) with manual annotation, and EVs were classified according to their morphology and electron density, as described (26, 27).

Phagocytosis and endocytosis assays

Uptake of naked nucleic acids was assessed microscopically by incubating adipocytes with rhodamine-conjugated p(dA:dT) or FITC-conjugated ODN 1668 CpG (both from InvivoGene) for 1 h. Endocytosis by means of pinocytosis was assessed by incubating adipocytes with FITC-conjugated dextran, followed by FACS analysis or fluorescence microscopy. Uptake of solid particles was assessed with the use of fluorescent latex beads (Sigma-Aldrich) and FACS analysis (BD LSR II).

ELISA assays

Tissue samples were weighed and homogenized in RIPA buffer using a Roche bead mill homogenizer at 6,500 rpm for 1 min. Cell culture supernatants and plasma samples were centrifuged at 0.8 g for 10 min to remove cell debris, and supernatants were used for analysis. We used commercial ELISA kits to measure the levels of IL-6, TNFα (Fisher Scientific), Vit-D3, calcitriol and VDR (MBS268259-48, MBS2701844-24, MyBioSource). All samples were stored at -80°C until analysis.

mtRNA isolation and *in vitro* transfection

Adipocyte mitochondria were isolated with a commercial mitochondrial isolation kit (Thermo Fisher Scientific, Waltham, MA). Mitochondrial RNA (mtRNA) was isolated by lysing the mitochondrial pellet with TRI Reagent (Sigma-Aldrich), as described (1). 3T3L1 cells were transfected with 2 μg of mtRNA in 6- or 24-well plates with cells at 80–90% confluency. As

a transfection reagent we used Lipofectamine 3000 (Invitrogen) at a 1:3 ratio. Control cells received transfection reagent only. Cells were analyzed 18 h after transfection.

mtDNA isolation and transfection

Mitochondrial DNA (mtDNA)was isolated from mitochondria pellets using TRI Reagent (Merck Sigma-Aldrich) and reconstituted in TE buffer (10 mM Tris-HCL, 1 mM EDTA, pH 8.0). 3T3L1 cells were transfected for 18 h with 1 µg/ml mtDNA using the TurboFect Transfection Reagent. Control cells received transfection reagent only. Agarose gel electrophoresis was used to examine mtDNA integrity.

Cytosolic mtRNA isolation

Cytosol fractions of 3T3-L1 preadipocytes were collected by subcellular fractionation of the cytoplasm and the cell organelles using digitonin, as described (45). Digitonin buffer contained 150 mM NaCl, 50 mM HEPES (pH 7.4) and 25 µg/ml digitonin (D141, Merck Sigma-Aldrich). Treated cells were processed until the step in which cytoplasm was obtained as described (1). 3T3-L1 cytoplasm (250 µl) was added to 750 µl TRI Reagent (T3934, Merck Sigma-Aldrich) and total RNA extraction was performed as described (24).

Histology and image analysis

Tissues were fixed with 4% paraformaldehyde and embedded in paraffin, as described (1). Sections were stained with hematoxylin and eosin (Carl Roth, Karlsruhe, Germany). Antibodies are listed in Supplemental Table 2. UCP1, IFI16, AIM2 and NPFFR1 immunohistochemistry was performed on paraffin-embedded tissue sections. For histomorphometry of fat cells we used Image J, with an image-processing algorithm that incorporated the Euclidean distance-based Watershed transformation to segment the images. Briefly, binarized images were generated using Otsu's method for thresholding; enhanced images were generated using contrast limited adaptive histogram equalization (CLAHE), and finally segmented images were generated using the Watershed transformation (Supplemental Figure 20). Negative control specimens of our fluorescent imaging and immunostaining are shown in Supplemental Figure 15. Mitochondrial content and morphology was analyzed with ImageJ, as described (14). Beige adipose area was measured with our custom-developed image analysis software (BeAR©, (14)).

Oil Red-O staining and quantification of UCP1 staining

The triglyceride content of cultured adipocytes was examined by Oil Red-O using a commercial kit from BioOptica (Milan, Italy), as described (24). *In vitro* UCP1 immunostaining was performed in 6-well culture plates, and samples were imaged and the optical density was measured using digital image analysis. Original images are available upon request through Figshare. Mitochondria were also labeled using an SDH-A histochemistry assay (BioOptica).

Adipocyte differentiation

Mouse preadipocytes of the stromal vascular fraction (SVF) were isolated and maintained as described (24, 43, 46). To ensure the depletion of adipose tissue macrophages (ATMs) from the harvested preadipocytes, we used magnetic bead cell purification of the SVF with an antibody against the F4/80 antigen (Miltenyi Biotec, Bergisch Gladbach, Germany) (47).

Human subcutaneous adipose tissue preadipocytes were harvested as described (24, 43). Preadipocytes were maintained in cell culture medium supplemented with 20 μg/mL insulin. To induce white differentiation of preadipocytes of the SVF, we treated the cells with 50 μM IBMX, 1 μM dexamethasone, 1 μM rosiglitazone and 20 μg/ml insulin (all from Merck Sigma-Aldrich), as described (14).

Flow cytometry analysis of DNA sensors, mitochondrial biogenesis, mitochondrial content and mitochondrial uncoupling

Mitochondrial content was analyzed with MitoTracker dyes (Thermo Fisher Scientific). Mitochondrial biogenesis was detected with the MitoBiogenesis™ Flow Cytometry Kit (Abcam, Cambridge, UK). MitoThermo Yellow (MTY), a temperature-sensitive fluorescent probe (48) was used to assess mitochondrial thermogenesis and uncoupling, as described (49, 50). Temperature difference between the control and the test groups was expressed as Mito-ΔT, and shown in the respective figures. MTY was developed and provided by Dr. Y-T. Chang (Center for Self-Assembly and Complexity, Institute for Basic Science & Department of Chemistry, Pohang University of Science and Technology, Pohang 37673, Republic of Korea). We used MTY for FACS analysis at 0.1 ng/ml to label 10^6/ml cells. Cells were maintained at 37°C throughout the assay. DNA sensors (STING, p204, AIM2, DDX41) were detected with unconjugated antibodies (listed in Supplemental Table 2) and labeled with an FITC-conjugated secondary antibody for FACS analysis. Nucleic acids were labeled with Sytox Green (Thermo Fisher). Flow Repository identifiers of raw FACS data are as follows: #FR-FCM-Z236, #FR-FCM-Z2R6, #FR-FCM-ZYPU, #FR-FCM-ZYUU.

Imaging of mitochondrial content, autophagy and lysosomes

For fluorescent microscopy of mitochondrial content and morphology preadipocytes or 3T3-L1 cells were grown on optical transparent glass-bottom plates (Greiner Bio-One GmbH, Frickenhausen, Germany) or glass coverslips. Functional mitochondria were labeled with MitoTracker Red. Mitochondria were also labeled with GFP using the BacMam 2.0 transfection system (Fisher Scientific). Oxygen consumption was assayed with the Extracellular O_2 Consumption Reagent (Abcam) for 30–120 min. Mitochondrial respiration was evaluated with the WST-81 assay (Carl Roth), as described (51). Autophagosomes and lysosomes were labeled with Cell Meter Autophagy Fluorescence Imaging kit (AAT Bioquest, Sunnyvale, CA), Lyso Brite Orange (Bertin Bioreagent, Montigny le Bretonneux, France) and Lyso View 405 (Biotium, Inc. Fremont, C). Inflammasome activity was measured with the Caspase-Glo 1 Inflammasome Assay (Promega Co., Madison, WI).

High fat diet feeding and indirect calorimetry

Respiratory exchange rate (RER), oxygen consumption (VO_2) and energy expenditure (EE) were measured in each individual mouse for 24 h using a small animal indirect calorimetry system (CaloBox, Phenosys, Germany). Mean RER, VO_2 and EE values were determined over 7 h in the middle of both the day and the night phases. Basal glucose levels and glucose tolerance were measured as described (24). For HFD feeding of mice (dams with litters P6 to P9, or mice at P28 for 12 weeks) we used a rodent HFD from SSNIFF Spezialdiäten (Soest,

Germany) (24). Vit-D3 was supplemented in diet, mtRNA was transfected with magnetofection for 14 days.

miRNA detection

Total RNA was extracted by TRIzol reagent (Invitrogen, Carlsbad, CA, USA) according to the manufacturer's instructions and was quantified using the NanoDrop™ 8000 Fluorospectrometer (Thermo Fisher Scientific). In total, 50 ng of purified RNA was subjected to reverse transcription using a TaqMan miRNA Reverse Transcription Kit and TaqMan® MicroRNA Assays (Applied Biosystems, Foster City, CA) according to the manufacturer's instructions (Assay ID: mmu-miR-434-3p, 002604; mmu-miR-29a-5p, 002447; RUN6B, 001973). Quantification of individual miRNAs was using a QuantStudio™ 12K flex real-time PCR system (Applied Biosystems) and the relative expression values were calculated by using the $2^{-\Delta\Delta Ct}$ method and normalized to *RUN6B*. miR434-3p was overexpressed using a custom-synthesized RNA (Sigma-Aldrich) and transfected with Turbofect transfection reagent (Fisher Scientific). To identify potential *Irf7*-interacting miRNA species, we searched the *TargetScan* database for miRNAs with complementarity to *Irf7* mRNA. In the next step, we used miRBase to identify precursor-, and mature sequences of the candidate miRNA species (52).

Cell viability assay

We used the Presto Blue Cell Viability Assay (Thermo Fisher Scientific) and the Rotitest Vital (Carl Roth) assays according to the manufacturers' instructions.

Western blotting

Cells were lysed in ice-cold RIPA buffer supplemented with Pierce™ protease and phosphatase inhibitor mini tablets (Thermo Scientific). Protein concentration was measured by the Pierce™ Rapid Gold BCA Protein Assay Kit and 30–40 µg protein samples were run on 16% SDS gels for protein separation, followed by blotting the gels on 0.2-µm nitrocellulose blotting membrane (Amersham, Freiberg, Germany) at 300 mA for 1 h in a cold room. After blotting, membranes were blocked with 5% skimmed milk for 1 h. Providers of the β-actin and LC3 antibodies are listed in Supplement Table 2. Antibody concentrations used were as follows: β-actin, 1:10,000, LC3, 0.2 µg/ml.

Quantification of nucleic acids in extracellular vesicles

We collected EV pellets from cells, from formula milk or infant formula in a clean Eppendorf tube, which was centrifuged at 0.8 g to remove cell debris. To isolate the EV-associated DNA from the pellets or from the cell culture media, we used the Zymo Quick DNA Microprep Kit (Zymo Research, Irvine, CA). After determination of the DNA concentration, we used 5 ng for qPCR assays. EV-depleted cell culture media was used as a reference. For comparison between groups, we used the ΔΔCt method to determine relative changes in mtDNA levels. For extraction of mtRNA and other EV-associated RNA species from cell EV pellets and culture media, we used Trizol Reagent. After determination of the RNA concentration, we used 50 ng of RNA to generate cDNA.

mtDNA copy number in the inguinal adipose tissue

We used Trizol Reagent DNA isolation from iAT at P6 and P56. DNA was reconstituted in TE buffer and adjusted to 10 ng/µl. We performed qPCR using *HK2* as a reference nuclear genome-encoded gene, and measured the DNA copy number of mtDNA-encoded 16S and Nd1. We calculated the copy number according to the formula:

$$\Delta Ct = Ct_{\text{Target gene}} - Ct_{\text{Reference gene}} \quad (1)$$
$$\text{mtDNA copy number} = 2X2^{(\Delta Ct)}$$

Magnetofection of mtRNA

In vivo delivery of mtRNA into the cytosol of adipocytes was achieved with magnetofection, using mtRNA–magnetic nanoparticle complexes (DogtorMag, OzBiosciences, San Diego, CA). Briefly, mtRNA-nanoparticle complexes were injected into the inguinal adipose tissue of mice, and enrichment of the magnetic nanoparticles was ensured by magnetic exposure of the fat depot, as described (53). MicroRNA was transfected using Lipofectamine 3000 (Thermo Fisher).

Institutional Review Board Statement

Research involving animals was approved by the regional governmental ethics and animal welfare committee in Tübingen, Germany (#1511; #1557; #1492; #1546; #o.232-1,2,4,5).

Acknowledgements for the supplemental information

The VDR inhibitor was provided by Prof. Dr. Leggy A. Arnold, University of Wisconsin, USA. MTY was developed and provided by Dr. Y-T. Chang (Center for Self-assembly and Complexity, Institute for Basic Science & Department of Chemistry, Pohang University of Science and Technology, Republic of Korea. The authors thank Prof. Hartmut Geiger (Ulm University) for providing access to the FACS equipment. The assistance of Katharina Schormair and Burak Yildiz in image analysis is much appreciated. The contribution of Vincent Pflüger, Yun Chen, Antonia Stubenvoll, Angelika Bauer are acknowledged. Elements of the 3D artwork used in the graphical abstract was provided by Dreamstime Stock Photography.

References

1. Seale P, Bjork B, Yang W, Kajimura S, Chin S, Kuang S, et al. PRDM16 controls a brown fat/skeletal muscle switch. *Nature.* 2008;454(7207):961-7.
2. Kissig M, Ishibashi J, Harms MJ, Lim H-W, Stine RR, Won K-J, et al. PRDM16 represses the type I interferon response in adipocytes to promote mitochondrial and thermogenic programing. *The EMBO Journal.* 2017;36(11):1528-42.
3. Seale P, Kajimura S, Yang W, Chin S, Rohas LM, Uldry M, et al. Transcriptional control of brown fat determination by PRDM16. *Cell metabolism.* 2007;6(1):38-54.
4. Jespersen NZ, Larsen TJ, Peijs L, Daugaard S, Homøe P, Loft A, et al. A classical brown adipose tissue mRNA signature partly overlaps with brite in the supraclavicular region of adult humans. *Cell Metab.* 2013;17(5):798-805.

5. Kozak LP. The genetics of brown adipocyte induction in white fat depots. *Front Endocrinol (Lausanne).* 2011;2:64.
6. Nascimento EBM, Sparks LM, Divoux A, van Gisbergen MW, Broeders EPM, Jörgensen JA, et al. Genetic Markers of Brown Adipose Tissue Identity and In Vitro Brown Adipose Tissue Activity in Humans. *Obesity.* 2018;26(1):135-40.
7. Perugini J, Bordoni L, Venema W, Acciarini S, Cinti S, Gabbianelli R, et al. Zic1 mRNA is transiently upregulated in subcutaneous fat of acutely cold-exposed mice. 2019;234(3):2031-6.
8. Pilkington A-C, Paz HA, and Wankhade UD. Beige Adipose Tissue Identification and Marker Specificity—Overview. *Front Endocrinol (Lausanne).* 2021;12(8).
9. Carobbio S, Rosen B, and Vidal-Puig A. Adipogenesis: new insights into brown adipose tissue differentiation. *Journal of molecular endocrinology.* 2013;51(3):T75-T85.
10. Sanchez-Gurmaches J, and Guertin DA. Adipocyte lineages: tracing back the origins of fat. *Biochim Biophys Acta.* 2014;1842(3):340-51.
11. Lee K-H, and Kim NH. Differential Expression of Adipocyte-Related Molecules in the Distal Epididymal Fat of Mouse during Postnatal Period. *Development & Reproduction.* 2019;23(3):213-21.
12. Hoang AC, Yu H, and Röszer T. Transcriptional Landscaping Identifies a Beige Adipocyte Depot in the Newborn Mouse. *Cells.* 2021;10(9):2368.
13. Rockstroh D, Landgraf K, Wagner IV, Gesing J, Tauscher R, Lakowa N, et al. Direct evidence of brown adipocytes in different fat depots in children. *PLOS ONE.* 2015;10(2):e0117841.
14. Yu H, Dilbaz S, Coßmann J, Hoang AC, Diedrich V, Herwig A, et al. Breast milk alkylglycerols sustain beige adipocytes through adipose tissue macrophages. *The Journal of Clinical Investigation.* 2019;129(6):2485-99.
15. Szklarczyk D, Gable AL, Lyon D, Junge A, Wyder S, Huerta-Cepas J, et al. STRING v11: protein-protein association networks with increased coverage, supporting functional discovery in genome-wide experimental datasets. *Nucleic acids research.* 2019;47(D1):D607-d13.
16. Luan Y, Lengyel P, and Liu C-J. p204, a p200 family protein, as a multifunctional regulator of cell proliferation and differentiation. *Cytokine Growth Factor Rev.* 2008;19(0):357-69.
17. Bourette RP, and Mouchiroud G. The biological role of interferon-inducible P204 protein in the development of the mononuclear phagocyte system. *Front Biosci.* 2008;13:879-86.
18. Choubey D, and Panchanathan R. Interferon-inducible Ifi200-family genes in systemic lupus erythematosus. *Immunol Lett.* 2008;119(1-2):32-41.
19. Tabula Muris C, Overall c, Logistical c, Organ c, processing, Library p, et al. Single-cell transcriptomics of 20 mouse organs creates a Tabula Muris. *Nature.* 2018;562(7727):367-72.
20. Ritchie C, Cordova AF, Hess GT, Bassik MC, and Li L. SLC19A1 Is an Importer of the Immunotransmitter cGAMP. *Molecular Cell.* 2019;75(2):372-81.e5.
21. Karikó K, Buckstein M, Ni H, and Weissman D. Suppression of RNA Recognition by Toll-like Receptors: The Impact of Nucleoside Modification and the Evolutionary Origin of RNA. *Immunity.* 2005;23(2):165-75.
22. Bakker P, Scantlebery A, Butter L, Claessen N, Teske G, Poll T, et al. TLR9 Mediates Remote Liver Injury following Severe Renal Ischemia Reperfusion. *PloS one.* 2015;10:e0137511.

23. Hines JH, Henle SJ, Carlstrom LP, Abu-Rub M, and Henley JR. Single vesicle imaging indicates distinct modes of rapid membrane retrieval during nerve growth. *BMC Biology.* 2012;10(1):4.
24. Waqas SFH, Hoang A, Lin Y, Ampem G, et al, and Röszer T. Neuropeptide FF increases M2 activation and self-renewal of adipose tissue macrophages. *The Journal of Clinical Investigation* 2017;127(7):2842-54.
25. Haag SM, Gulen MF, Reymond L, Gibelin A, Abrami L, Decout A, et al. Targeting STING with covalent small-molecule inhibitors. *Nature.* 2018;559(7713):269-73.
26. Waldenström A, Gennebäck N, Hellman U, and Ronquist G. Cardiomyocyte Microvesicles Contain DNA/RNA and Convey Biological Messages to Target Cells. *PloS one.* 2012;7:e34653.
27. Zabeo D, Cvjetkovic A, Lässer C, Schorb M, Lötvall J, and Höög JL. Exosomes purified from a single cell type have diverse morphology. *Journal of extracellular vesicles.* 2017;6(1):1329476-.
28. Durcin M, Fleury A, Taillebois E, Hilairet G, Krupova Z, Henry C, et al. Characterisation of adipocyte-derived extracellular vesicle subtypes identifies distinct protein and lipid signatures for large and small extracellular vesicles. *Journal of extracellular vesicles.* 2017;6(1):1305677.
29. Ragni E, Perucca Orfei C, De Luca P, Viganò M, Colombini A, Lugano G, et al. miR-22-5p and miR-29a-5p Are Reliable Reference Genes for Analyzing Extracellular Vesicle-Associated miRNAs in Adipose-Derived Mesenchymal Stem Cells and Are Stable under Inflammatory Priming Mimicking Osteoarthritis Condition. *Stem Cell Reviews and Reports.* 2019;15(5):743-54.
30. Datta A, Kim H, McGee L, Johnson AE, Talwar S, Marugan J, et al. High-throughput screening identified selective inhibitors of exosome biogenesis and secretion: A drug repurposing strategy for advanced cancer. *Scientific Reports.* 2018;8(1):8161.
31. Zitomer NC, Mitchell T, Voss KA, Bondy GS, Pruett ST, Garnier-Amblard EC, et al. Ceramide synthase inhibition by fumonisin B1 causes accumulation of 1-deoxysphinganine: a novel category of bioactive 1-deoxysphingoid bases and 1-deoxydihydroceramides biosynthesized by mammalian cell lines and animals. *The Journal of biological chemistry.* 2009;284(8):4786-95.
32. Narvaez CJ, Matthews D, Broun E, Chan M, and Welsh J. Lean phenotype and resistance to diet-induced obesity in vitamin D receptor knockout mice correlates with induction of uncoupling protein-1 in white adipose tissue. *Endocrinology.* 2009;150(2):651-61.
33. Lorenz R, Bernhart SH, Höner Zu Siederdissen C, Tafer H, Flamm C, Stadler PF, et al. ViennaRNA Package 2.0. *Algorithms for molecular biology : AMB.* 2011;6:26.
34. Hornung V, Ellegast J, Kim S, Brzózka K, Jung A, Kato H, et al. 5'-Triphosphate RNA Is the Ligand for RIG-I. *science.* 2006;314(5801):994-7.
35. Kato H, Takeuchi O, Mikamo-Satoh E, Hirai R, Kawai T, Matsushita K, et al. Length-dependent recognition of double-stranded ribonucleic acids by retinoic acid-inducible gene-I and melanoma differentiation-associated gene 5. *The Journal of experimental medicine.* 2008;205(7):1601-10.
36. Ablasser A, Bauernfeind F, Hartmann G, Latz E, Fitzgerald KA, and Hornung V. RIG-I-dependent sensing of poly(dA:dT) through the induction of an RNA polymerase III–transcribed RNA intermediate. *Nature Immunology.* 2009;10(10):1065-72.
37. Stoppelenburg AJ, von Hegedus JH, Huis in't Veld R, Bont L, and Boes M. Defective control of vitamin D receptor-mediated epithelial STAT1 signalling predisposes to severe respiratory syncytial virus bronchiolitis. *The Journal of Pathology.* 2014;232(1):57-64.

38. Cippitelli M, and Santoni A. Vitamin D3: a transcriptional modulator of the interferon-γ gene. *European Journal of Immunology.* 1998;28(10):3017-30.
39. Helming L, Böse J, Ehrchen J, Schiebe S, Frahm T, Geffers R, et al. 1α,25-dihydroxyvitamin D3 is a potent suppressor of interferon γ–mediated macrophage activation. *Blood.* 2005;106(13):4351-8.
40. Das M, Tomar N, Sreenivas V, Gupta N, and Goswami R. Effect of vitamin D supplementation on cathelicidin, IFN-γ, IL-4 and Th1/Th2 transcription factors in young healthy females. *European Journal of Clinical Nutrition.* 2014;68(3):338-43.
41. Unterholzner L, Keating SE, Baran M, Horan KA, Jensen SB, Sharma S, et al. IFI16 is an innate immune sensor for intracellular DNA. *Nature immunology.* 2010;11(11):997-1004.
42. Sidhu PS, Teske K, Feleke B, Yuan NY, Guthrie ML, Fernstrum GB, et al. Anticancer activity of VDR-coregulator inhibitor PS121912. *Cancer Chemother Pharmacol.* 2014;74(4):787-98.
43. Waqas SFH, Noble A, Hoang A, Ampem G, Popp M, Strauß S, et al. Adipose tissue macrophages develop from bone marrow-independent progenitors in *Xenopus laevis* and mouse. *Journal of Leukocyte Biology.* 2017;102(3):845-55.
44. De Carlo S, and Harris JR. Negative staining and cryo-negative staining of macromolecules and viruses for TEM. *Micron.* 2011;42(2):117-31.
45. Holden P, and Horton WA. Crude subcellular fractionation of cultured mammalian cell lines. *BMC research notes.* 2009;2:243.
46. Hausman DB, Park HJ, and Hausman GJ. Isolation and culture of preadipocytes from rodent white adipose tissue. *Methods in molecular biology.* 2008;456:201-19.
47. Ampem G, and Röszer T. In: Badr MZ ed. *Nuclear Receptors: Methods and Experimental Protocols*. New York, NY: Springer New York; 2019:225-36.
48. Arai S, Suzuki M, Park SJ, Yoo JS, Wang L, Kang NY, et al. Mitochondria-targeted fluorescent thermometer monitors intracellular temperature gradient. *Chemical communications.* 2015;51(38):8044-7.
49. Lane N. Hot mitochondria? *PLoS biology.* 2018;16(1):e2005113.
50. Chrétien D, Bénit P, Ha H-H, Keipert S, El-Khoury R, Chang Y-T, et al. Mitochondria are physiologically maintained at close to 50 °C. *PLoS biology.* 2018;16(1):e2003992.
51. Karabatsiakis A, Böck C, Salinas-Manrique J, Kolassa S, Calzia E, Dietrich DE, et al. Mitochondrial respiration in peripheral blood mononuclear cells correlates with depressive subsymptoms and severity of major depression. *Translational Psychiatry.* 2014;4(6):e397-e.
52. Agarwal V, Bell GW, Nam J-W, and Bartel DP. Predicting effective microRNA target sites in mammalian mRNAs. *eLife.* 2015;4:e05005.
53. Plank C, and Rosenecker J. Magnetofection: The Use of Magnetic Nanoparticles for Nucleic Acid Delivery. *Cold Spring Harbor Protocols.* 2009;2009(6):pdb.prot5230.

Supplementary Files

This is a list of supplementary files associated with this preprint. Click to download.

- HoangSupplementaryInformation.pdf